nature medicine

Article

https://doi.org/10.1038/s41591-025-04186-5

Fecal microbiota transplantation plus immunotherapy in non-small cell lung cancer and melanoma: the phase 2 FMT-LUMINate trial

Received: 24 July 2025

Accepted: 18 December 2025

Published online: 28 January 2026

Check for updates

A list of authors and their affiliations appears at the end of the paper

Immune checkpoint inhibitors (ICI) have improved outcomes for patients with non-small cell lung cancer (NSCLC) and melanoma, yet over half of patients exhibit primary resistance. Fecal microbiota transplantation (FMT) may overcome resistance to anti-programmed cell death protein 1 (PD-1) therapy. The clinical activity and safety of FMT plus anti-PD-1 in NSCLC or anti-PD-1 plus anti-cytotoxic T-lymphocyte antigen 4 (CTLA-4) therapy in melanoma have not been evaluated. Here we report results from FMT-LUMINate, a multicenter, open-label, phase 2 trial assessing healthy donor FMT plus anti-PD-1 in NSCLC ($n = 20$) or anti-PD-1 plus anti-CTLA-4 (dual ICI) in melanoma ($n = 20$), in the first-line setting. Eligible patients received a single FMT via oral capsules prior to ICI initiation. The primary endpoint was objective response rate (ORR) in NSCLC. Secondary endpoints included ORR in melanoma, safety and donor–host microbiome similarity. In NSCLC, the ORR was 80% (16/20), meeting the study primary endpoint. In melanoma, the ORR was 75% (15/20). FMT was deemed safe in both cohorts by an independent data and safety monitoring committee, with no grade 3 or higher adverse events (AEs) in NSCLC and 13 (65%) patients experiencing grade 3 or higher AEs in melanoma. Shotgun metagenomic sequencing revealed that responders developed a distinct post-FMT gut microbiome composition, independent of acquired donor–recipient similarity or strain-level engraftment. Responders exhibited significantly greater loss of baseline bacterial species compared to non-responders, with frequent depletion of *Enterocloster citroniae*, *E. lavalensis* and *Clostridium innocuum*. This finding was reproduced across three published FMT oncology trials. We recolonized antibiotic-treated, tumor-bearing mice with post-FMT stool from two responder patients, and reintroduction of the specific bacterial species that were lost after FMT abrogated the antitumor effect of ICI. Taken together, these findings confirm the clinical activity of FMT in combination with ICI and suggest that the elimination of deleterious taxa is required for FMT-mediated therapeutic benefit. ClinicalTrials.gov identifier: NCT04951583.

e-mail: arielle.elkrief@umontreal.ca

Immune checkpoint inhibitors (ICI) have improved therapeutic outcomes for patients with NSCLC[1] and cutaneous melanoma (herein referred to as melanoma)[2]. Patients with NSCLC and tumor proportion score (TPS) PD-L1 ≥ 50%, in the absence of a first-line actionable oncogenic alteration, are treated with single-agent anti-PD-1 such as pembrolizumab, with an expected objective response rate (ORR) of 39–45%[1,3,4]. In patients with melanoma, dual therapy with ipilimumab (anti-CTLA-4) in combination with nivolumab (anti-PD-1) is among the most commonly used frontline regimens, yielding an ORR of 50–58% and durable improvements in overall survival (OS) compared to single-agent ipilimumab[2]. Despite improvements in OS, approximately half of patients will not respond to these regimens[5], highlighting an urgent need to improve the efficacy of ICI. Over the past decade, the gut microbiota has emerged as one of the hallmarks of cancer and as a key determinant of response to ICI[6–12]. First, preclinical studies demonstrated that FMT from non-responder (NR) patients induced resistance to anti-CTLA-4 (ref. 7) or anti-PD-(L)-1 (refs. 6,8–10) therapy in murine models, and response to ICI was restored after FMT from responder (R) patients[13]. Gut microbiota sequencing of stool samples from clinical cohorts of patients with solid tumors has demonstrated that enrichment of potentially deleterious bacteria, including *Enterocloster* and *Clostridium* spp., were associated with resistance to ICI[14,15]. This dysbiosis can be further compounded by iatrogenic insults such as antibiotics[16–19], now validated as an independent negative prognostic factor across multiple oncology settings. Subsequently, two phase 1 clinical trials demonstrated the first proof of concept that FMT from patients with response to anti-PD-1 could overcome primary or acquired resistance to ICI[20–22]. Soon thereafter, the phase 1 MIMIC trial demonstrated the potential of healthy donor FMT to decrease primary resistance to anti-PD-1 therapy in patients with melanoma[23,24]. However, the clinical activity of FMT in combination with ICI in patients with NSCLC remains unknown. In addition, the safety and clinical activity of FMT in combination with anti-PD-1 plus anti-CTLA-4 in patients with melanoma has not been described. Moreover, the mechanism by which FMT enhances the activity of ICI in humans remains poorly understood. Here we report the clinical activity of FMT combined with anti-PD-1 in patients with NSCLC and with anti-PD-1 plus anti-CTLA-4 in patients with melanoma. We also describe how the loss of deleterious bacteria prevalent at baseline—but no longer detected after FMT—may modulate the therapeutic effects of FMT when combined with ICI.

Results

FMT increases the clinical activity of anti-PD-1 in NSCLC and anti-PD-1 plus anti-CTLA-4 in melanoma

A total of 59 patients were screened for eligibility between 18 November 2021 and 6 March 2024 (Fig. 1a), of whom 20 were enrolled in the NSCLC cohort and 20 were enrolled in the melanoma cohort. The primary endpoint was ORR in the NSCLC cohort. The secondary endpoints were progression-free survival (PFS) at 1 year, OSat 1 year, disease control rate (DCR) and duration of response in the NSCLC and cutaneous melanoma cohorts, ORR in the cutaneous melanoma cohort, safety of FMT with ICI and acquired donor–host similarity as measured by the Bray–Curtis dissimilarity index[25]. Endpoints in the uveal melanoma cohort were exploratory and, therefore, are reported separately (see 'Outcomes and sample size' in the Methods).

Patients in the NSCLC cohort were enrolled if they had no first-line actionable oncogenic alterations, PD-L1 TPS ≥ 50% and no prior exposure to anti-PD-1 therapy. Patients in the melanoma cohort were enrolled irrespective of $BRAF^{V600}$ mutational status, and prior adjuvant anti-PD-1 was permitted, provided the last dose was administered more than 6 months prior to enrollment. Full inclusion and exclusion criteria are reported in the Methods. Patients underwent single FMT from a healthy donor delivered by oral capsules, administered the day after bowel preparation with polyethylene glycol (PEG) laxative and within 1 week before first-line anti-PD-1 monotherapy (pembrolizumab) in the NSCLC cohort or dual anti-PD-1 plus anti-CTLA-4 (nivolumab and ipilimumab) in the melanoma cohort (Extended Data Fig. 1a). Ten individual healthy donor volunteers provided feces, with 10 donors participating in the NSCLC cohort and six donors participating in the melanoma cohort (Extended Data Fig. 1b), with donor demographics presented in Supplementary Table 1.

Baseline characteristics for the enrolled patients are presented in Table 1. For the NSCLC cohort, median age was 68 (range 52–82) years, and 11 (55%) patients were male. Sixteen (80%) patients had adenocarcinoma histology, and 18 (90%) patients had stage IV disease, with two (10%) harboring unresectable stage III disease not amenable to curative-intent therapy. Twelve (60%) patients had PD-L1 TPS < 90%. For the melanoma cohort, median age was 56 (range 27–88) years, and 13 (65%) were male. Nine (45%) patient tumors harbored $BRAF^{V600}$ mutations. No patients were treated with BRAF/MEK inhibition for metastatic disease prior to enrollment. Seventeen (85%) patients had stage IV disease, including six (30%) with liver metastases at baseline and two (10%) with brain metastases at baseline. Median follow-up for the study was 24 months. The primary endpoint for this study was ORR in NSCLC. The ORR in the NSCLC cohort was 80% (95% confidence interval: 58.4–91.9), with 16 patients experiencing a partial response, exceeding the prespecified primary endpoint of 64% and, thereby, meeting the criteria for a positive study outcome (Fig. 1b,c). The DCR in NSCLC was 95% (three of four patients who did not achieve response experienced stable disease ≥6 months) (Fig. 1b,c). The median duration of response was 8.7 months (95% confidence interval: 3.1–20). The PFS and OS at 1 year were 65% (95% confidence interval: 47.1–89.7) and 100%, respectively (95% confidence interval not evaluable) (Extended Data Fig. 2a,b).

A key secondary endpoint of the study was activity of FMT in combination with anti-PD-1 plus anti-CTLA-4 in the melanoma cohort. The ORR in the melanoma cohort was 75% (95% confidence interval: 53.1–88.8), with 11 partial responses and four complete responses (Fig. 1d,e). The DCR was also 75% (Fig. 1d,e). The median duration of response was 10 months (95% confidence interval: 0–20.9). The PFS and OS at 1 year were 58% (95% confidence interval: 39.4–85.4) and 79% (95% confidence interval: 62.9–99.6), respectively (Extended Data Fig. 2c,d). These results demonstrate clinical efficacy of FMT in combination with anti-PD-1 therapy in NSCLC and with anti-PD-1 plus anti-CTLA-4 in melanoma.

FMT in combination with anti-PD-1 or anti-PD-1 plus anti-CTLA-4 was safe, with earlier onset of toxicity observed with dual ICI

FMT alone prior to ICI initiation resulted in grade 1 AEs in 35% of patients, most commonly diarrhea and changes in stool appearance, consistent with our previously published phase 1 trial[23] (Extended Data Table 1). No patient experienced previously unreported AEs related to FMT or to ICI. In the NSCLC cohort, any-grade AEs attributable to FMT plus anti-PD-1 occurred in 17 (85%) patients, and no patients experienced grade 3 or higher AEs. Corticosteroids were used in three (15%) patients for grade 2 AEs (arthritis, pancreatitis and pneumonitis). One patient who experienced grade 2 pneumonitis discontinued therapy due to this AE; however, this patient was symptom free with continued response maintained at last follow-up. One patient with grade 2 arthritis was treated with subsequent hydroxychloroquine and methotrexate. This patient was also symptom free with continued response at last follow-up. In the melanoma cohort, any-grade AEs related to FMT plus anti-PD-1 plus anti-CLTA-4 occurred in 19 (95%) patients, and 12 (60%) patients experienced grade 3 AEs and one patient experienced a grade 4 AE. The most frequent grade 3 or higher AE was diarrhea or colitis, occurring in 20% of patients. Three (15%) patients experienced myocarditis. Additional details on the myocarditis cases are presented in Supplementary Table 2. Thirteen (65%) patients in the melanoma cohort required corticosteroids for AEs. Two (10%) patients required second-line immunosuppression (one patient was treated

https://doi.org/10.1038/s41591-025-04186-5

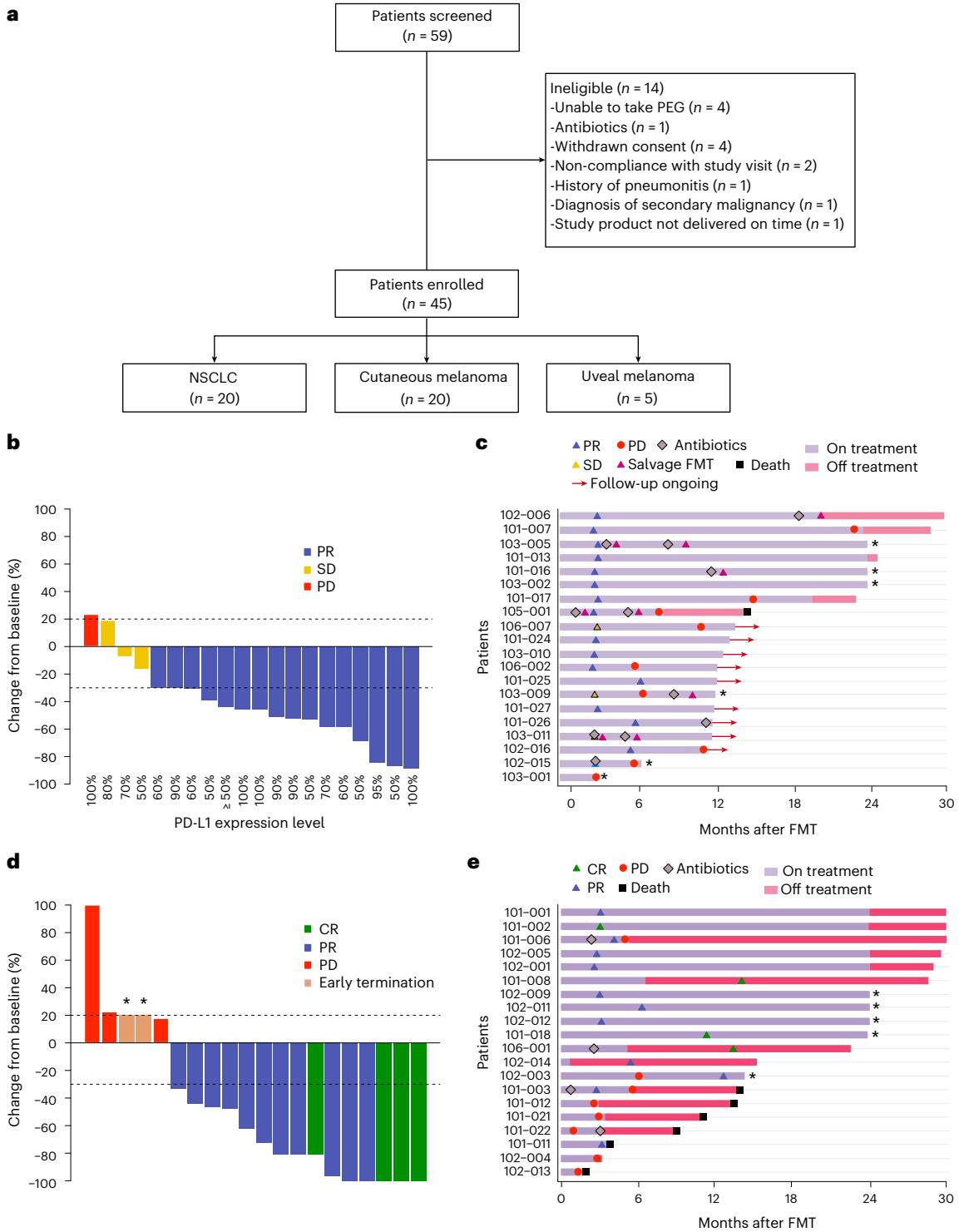

Fig. 1 | Clinical efficacy of FMT in combination with ICI in patients with previously untreated NSCLC and melanoma. a, Patient enrollment diagram. **b**–**c**, Waterfall plot showing the best objective response, with PD-L1 tumor expression shown for each patient on the horizontal axis (**b**) and swimmer plot showing the time-on-treatment after FMT in combination with pembrolizumab in $n = 20$ patients with NSCLC (**c**). **d**–**e**, Waterfall plot showing the best objective response (**d**) and swimmer plot showing the time-on-treatment after FMT in combination with ipilimumab plus nivolumab in $n = 20$ patients with melanoma (**e**). CR, complete response; PD, progressive disease; PR, partial response; SD, stable disease. Asterisks in the swimmer plot indicate that ICI treatment was discontinued at the moment of last-follow-up. Dashed lines in the waterfall plot at −30% indicate at least PR, and dashed lines in the waterfall plot at +20% indicate PD. Asterisks in the waterfall plot indicate disease progression due to clinical progression or death. PD-L1, programmed death ligand 1.

with infliximab for grade 3 diarrhea, and one patient was treated with infliximab and plasmapheresis for grade 4 myocarditis). The median onset of grade 3 or higher AEs was 40 days from the start of anti-PD-1 and anti-CLTA-4. Fourteen (70%) patients in the melanoma cohort discontinued ICI due to toxicity, and six (30%) patients completed all four cycles of anti-PD-1 plus anti-CTLA-4. The combination of FMT with ICI in both cohorts was deemed safe by an independent data safety and monitoring committee (DSMC) with AEs consistent with known

https://doi.org/10.1038/s41591-025-04186-5

Table 1 | Baseline characteristics

NSCLC		
Characteristic	**Total cohort (*N*=20)[a]**	
Age at diagnosis, years	68	(52–82)
Sex		
Male	11	(55%)
Female	9	(45%)
Race		
White	20	(100%)
BMI, kg m^{-2}		
BMI<30	15	(75%)
BMI≥30	5	(25%)
ECOG performance status		
0	10	(50%)
1	9	(45%)
2	1	(5%)
Stage		
IV	18	(90%)
III	2	(10%)
NSCLC histology		
Adenocarcinoma	16	(80%)
Squamous cell carcinoma	4	(20%)
Smoking history		
Former	15	(75%)
Current	4	(20%)
Never	1	(5%)
PD-L1		
PD-L1<90%	12	(60%)
PD-L1≥90%	8	(40%)
Baseline brain metastases		
Absent	19	(95%)
Present	1	(5%)
Prior anti-PD-1	6	(30%)
Melanoma		
Characteristic	**Total cohort (*N*=20)[a]**	
Age at diagnosis, years	56	(27–88)
Sex		
Male	13	(65%)
Female	7	(35%)
Race		
White	20	(100%)
BMI, kg m^{-2}		
BMI<30	11	(55%)
BMI≥30	9	(45%)
ECOG performance status		
0	17	(85%)
1	2	(10%)
2	1	(5%)
Stage		
IV	17	(85%)
III	3	(15%)
M1 staging		
M1a	8	(40%)
M1c	7	(35%)
M1b	3	(15%)
M1d	2	(10%)
BRAF		
Wild-type	10	(50%)
Mutant	9	(45%)
Unknown	1	(5%)
BRAF status type		
Wild-type	10	(50%)
V600E	8	(40%)
K601E	1	(5%)
Not applicable	10	(50%)
LDH	8	(40%)
LDH normal	1	(5%)
LDH>upper limit of normal	1	(5%)
Baseline brain metastases		
Absent	17	(85%)
Present	3	(15%)
Baseline liver metastases		
Absent	18	(90%)
Present	2	(10%)
Prior adjuvant anti-PD-1 therapy		
No prior anti-PD-1	14	(70%)
Prior anti-PD-1	6	(30%)

LDH, lactate dehydrogenase, BMI, body mass index, ECOG, Eastern Cooperative Oncology Group. [a]Median (minimum–maximum); *n* (%).

toxicity profile of ipilimumab plus nivolumab, in accordance with the predefined safety criteria outlined in the protocol; however, the DSMC concluded that severe AEs reported in the melanoma cohort had an earlier onset than previously reported in the literature[26]. Additionally, myocarditis was deemed an AE of special interest for monitoring in future FMT trials.

Engraftment of donor-specific *Prevotella* spp. is associated with the development of immunotherapy-related AEs in the context of anti-CTLA-4 backbone

Given the accelerated onset of AEs and potential signal for increased incidence of myocarditis only in the dual anti-PD-1 plus anti-CTLA-4-treated melanoma cohort, we investigated these potential adverse safety signals by exploring the association between donor and development of AEs. Among the 13 patients who experienced grade 3 or higher AEs, six were attributed to donor 5 (Extended Data Fig. 3a). Moreover, all the fecal donations provided by donor 5 led to grade 3 or higher AEs in the melanoma cohort (Extended Data Fig. 3a). Additionally, two out of the three patients who experienced myocarditis received FMT from donor 5 (Supplementary Table 2). The two patients who developed myocarditis after receiving FMT from donor 5 experienced myocarditis of rapid onset (22 days and 25 days, respectively, after the first dose of ICI), compared to a relatively delayed onset (205 days) observed in the third patient who received FMT from donor 9.

Due to the relatively high number of healthy donors used in our study, we performed unsupervised clustering of donor gut microbiota composition and observed two distinct donor clusters ($P = 0.001$) (Fig. 2a), also observed in the NSCLC and melanoma cohorts when analyzed separately (Supplementary Fig. 1a,b). Cluster B, comprising samples from donor 5 and donor 11, was characterized by high relative abundance of *Prevotella* spp., including *Segatella copri* (previously *Prevotella copri* clade A), *Prevotella* sp. *Marseille-P4119*, *Prevotella stercorea* and an unknown species in the Prevotellaceae family (SGB1472) (Fig. 2b and Extended Data Fig. 3a), also observed in each cohort when analyzed separately (Supplementary Fig. 1c,d). Conversely, cluster A, consisting of the remaining donors, contained primarily other taxa (Fig. 2b) as well as a significantly lower relative abundance of *Prevotella* spp. compared to cluster B (Extended Data Fig. 3b). Differential abundance analysis comparing patients who developed grade 3 or higher AEs confirmed that *P.* sp. *Marseille-P4119*, *P. stercorea* and *Prevotellaceae* GGB1146 SGB1472 were enriched in patients who developed grade 3 or higher AEs (Fig. 2c). *S. copri*, *P.* sp. *Marseille-P4119* and *P. stercorea* were enriched after FMT compared to baseline in the patients who experienced grade 3 or higher AEs (Fig. 2d). Post-FMT engraftment at the sample level of *P.* sp. *Marseille-P4119*, *P. stercorea* and *Prevotellaceae* SGB1472 was associated with grade 3 or higher AEs ($P < 0.001$, $P = 0.023$ and $P < 0.001$, respectively, using Fisher's exact test). Patients without signs of severe toxicity did not exhibit enrichment of *Prevotella* spp. after FMT (Extended Data Fig. 3c).

Donor 5 was a *Prevotella*-rich donor who had participated in our previously published phase 1 study (MIMIC) involving patients with melanoma treated with FMT and monotherapy anti-PD-1, in which five (25%) patients experienced grade 3 or higher AEs[23]. However, donor 5 feces did not lead to toxicity in these anti-PD-1 monotherapy-treated patients. Moreover, FMT from *Prevotella*-rich donors was not associated with grade 3 or higher AEs in patients with NSCLC (Extended Data Fig. 3a). An analysis including all patients who experienced grade 3 or higher AEs in our current study and previously published phase 1 study[23] revealed that feces from cluster B donors caused toxicity only in patients receiving dual PD-1 and CTLA-4 blockade ($P = 0.051$) (Fig. 2e,f), with increased proportion of a subset of $CD4^+$ T cells in the peripheral blood after FMT in those who developed grade 3 or higher AEs ($P = 0.026$). (Supplementary Fig. 2a). Engraftment of *S. copri* was associated with these $CD4^+$ T cells in patients who were treated with dual PD-1 and CTLA-4 blockade and not in the context of single-agent ICI (Supplementary Fig. 2b). Of note, although there was a numerical association between the development of grade 3 or higher AEs and clinical response (Extended Data Fig. 3d), these results were not statistically significant. There was no association between the engraftment of *Prevotella* spp. and response ($P > 0.05$ for all *Prevotella* spp. using Fisher's exact test). Taken together, these results highlight that the gut microbiome—specifically, engraftment of donor-specific *Prevotella* spp.—was associated with the development of immune-related AEs in the context of dual immune checkpoint inhibition.

Post-FMT shift in the gut microbiome in R patients is not dictated by acquired donor similarity or donor strain engraftment

We next explored the impact of the donor on the efficacy of FMT and ICI. Unlike the donor effect that we observed with respect to AEs, no donor effect was detected with respect to efficacy—each donor, or donor cluster, led to a proportional number of responses and non-responses (Extended Data Figs. 3a and 4a). We next explored microbiome features associated with clinical outcomes. Alpha (α) diversity as measured by the Shannon index[27]—which measures the number of species (richness) and their relative abundances (evenness)—was similar between the healthy donors and patients at baseline in the NSCLC and melanoma groups (Extended Data Fig. 4b). Beta (β) diversity[28]—which measures the differences in microbial composition between samples—did not differ significantly between the R patients and the NR patients at baseline in the NSCLC ($P = 0.4$) and melanoma ($P = 0.9$) groups (Fig. 3a,b). After FMT, although there was no difference in α-diversity between R patients and NR patients (Extended Data Fig. 4b), we observed response-associated shifts in the global microbiota composition in both the NSCLC ($P = 0.09$) and melanoma ($P = 0.006$) cohorts (Fig. 3a,b).

We next computed the Bray–Curtis dissimilarity index[23,25], which measures the acquired degree of similarity between the recipient patients and their matching donor. No significant differences were observed between R patients and NR patients, indicating similar levels of donor microbiota acquisition according to response status (Extended Data Fig. 4c). We next explored strain-level engraftment using the StrainPhlAn pipeline[29] as described in Methods, which measures specific subspecies (strains) that engrafted from the corresponding donor. Both R patients and NR patients exhibited effective strain-level engraftment from donors with no significant difference in absolute number of strains engrafted between R and NR (Extended Data Fig. 4d). These results suggest that the global shift distinguishing R patients from NR patients observed after FMT was not driven by acquired donor–host similarity or strain engraftment from the donor.

Next, we examined species-level differential abundance between R patients and NR patients after FMT. In NSCLC R, we observed enrichment of beneficial bacteria[14,30,31], including *Faecalibacterium prausnitzii*, *Gemmiger formicilis* and *Akkermansia muciniphila*, after FMT, whereas enrichment of deleterious bacteria such as *Streptococcus vestibularis* and *Fusobacterium nucleatum* occurred in NR (Fig. 3c). The terminology 'beneficial' versus 'deleterious' refers to bacterial classification described in recent articles[14,30,32–35] as associated with a 'healthy' or 'immunosensitive' status versus a diseased or immunoresistant status (including cancer and any chronic inflammatory disorders, respectively). In the case of melanoma R patients, we observed a relative enrichment of *Bacteroides eggerthii*, *Bacteroides faecis* and *Alistipes senegalensis* after FMT compared to NR patients (Fig. 3d). In both NSCLC and melanoma R patients, we observed a relative enrichment in Oscillospiraceae (also called 'Ruminococcaceae') family members after FMT, consistent with their previously reported association with favorable ICI response[30,35,36] (Fig. 3e,f). Among R patients, a concomitant relative depletion of deleterious bacteria[14,30,31], including *E. lavalensis*, *Clostridium scindens* and *C. innocuum*, was observed after FMT compared to baseline (Fig. 3e,f). Aside from Firmicutes SGB15368, there was no overlap in enriched species between NSCLC and melanoma R patients after FMT (Extended Data Fig. 4e). Altogether, these results indicate that the post-FMT shift in the gut microbiome in R patients was not dictated by acquired donor–host similarity or strain engraftment from the donor, with limited overlap of enrichment of beneficial species after FMT in the NSCLC and melanoma cohorts.

Loss of deleterious bacterial species from the patient at baseline mediates the response to FMT

To better understand the taxonomic drivers of clinical outcome and the global shift in the microbiome distinguishing R from NR after FMT, we next examined changes in the absolute number of species-level genome bins (SGBs, metagenomically inferred microbial taxa approximating species-level resolution)[37] across key categories: (1) present uniquely in the donor, (2) present uniquely in the patient at baseline, (3) present in the patient at baseline and the donor, (4) lost SGBs relative to the SGBs detected in the patient at baseline and (5) new SGBs that were neither detected in the patient at baseline nor derived from the donor (Fig. 4a,b). Although the number of SGBs engrafted from the donor was similar in R patients versus NR patients ($P = 0.15$) (Extended Data Fig. 5a), we noted that the magnitude of SGB loss calculated from the patient at baseline was significantly higher in R compared to NR after FMT ($P = 0.016$) (Fig. 4c). The magnitude of SGBs loss from baseline in R patients was maintained in both NSCLC

https://doi.org/10.1038/s41591-025-04186-5

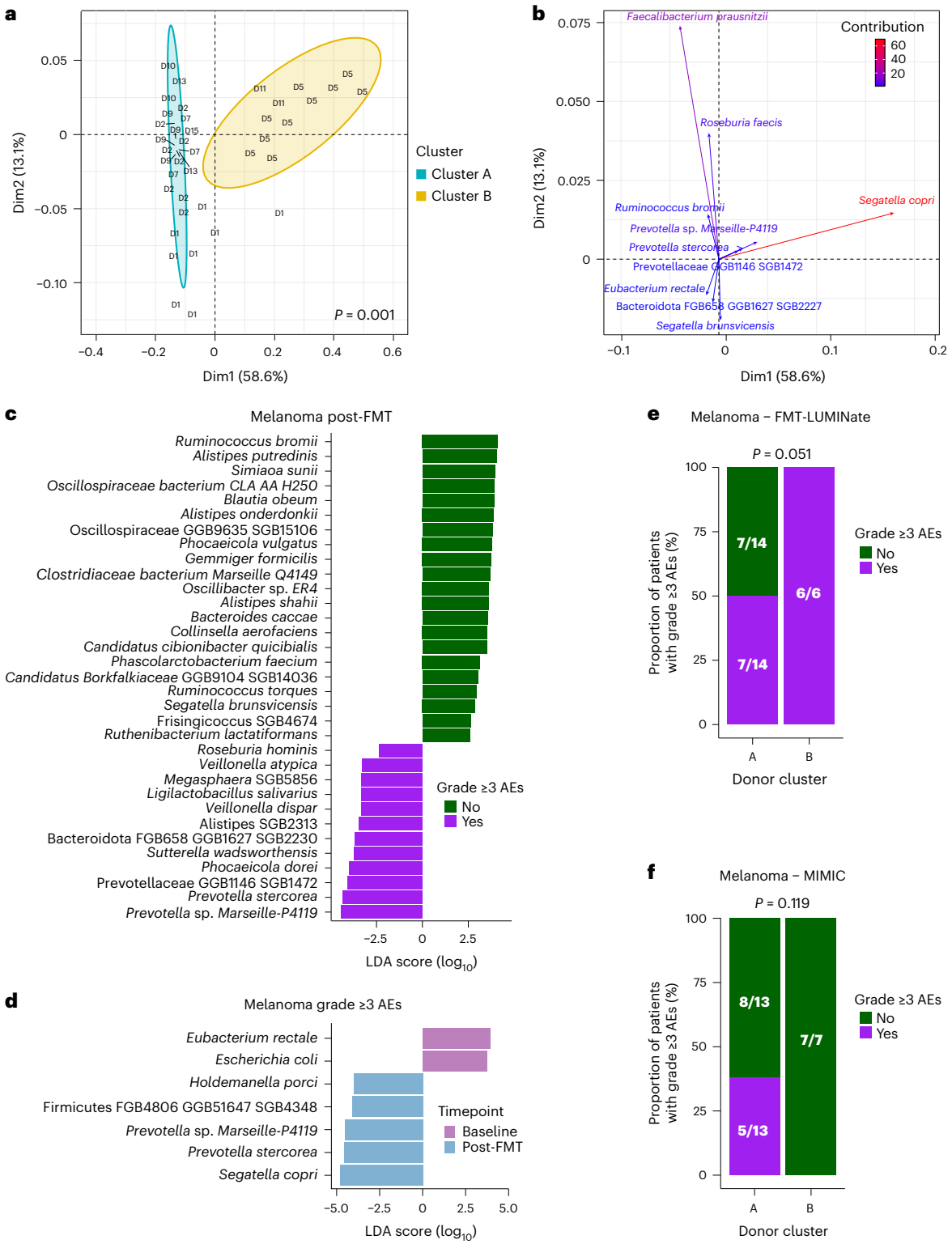

Fig. 2 | Relationship between the gut microbiome and grade 3 or higher immune-related AEs. a, Unsupervised cluster analysis using shotgun metagenomic sequencing of healthy donors using Bray–Curtis index ($n = 41$ samples from nine donors); group separation was assessed using PERMANOVA. **b**,Contribution of species driving donor clusters ($n = 41$ samples from nine donors). **c**, LDA using LEfSe (bar plot representing the $\log_{10}$ transformation of the LDA score) comparing post-FMT samples from patients with grade 3 or higher AEs to those from patients without grade 3 or higher AEs ($n = 79$ samples from 20 patients). **d**, LDA using LEfSe (bar plot representing the $\log_{10}$ transformation of the LDA score) of baseline compared to 1 month after FMT among patients with grade 3 or higher AEs ($n = 23$ samples from 12 patients). Significant values had linear discriminant analysis (LDA) scores greater than 2 and $P < 0.05$. **e**–**f**, Bar plot representation comparing proportion of patients who developed grade 3 or higher AEs according to donor cluster for FMT-LUMINate patients with melanoma (**e**) and for MIMIC patients with melanoma (**f**). Group differences were assessed using Fisher's exact test (two-sided). D, donor; Dim, dimension.

https://doi.org/10.1038/s41591-025-04186-5

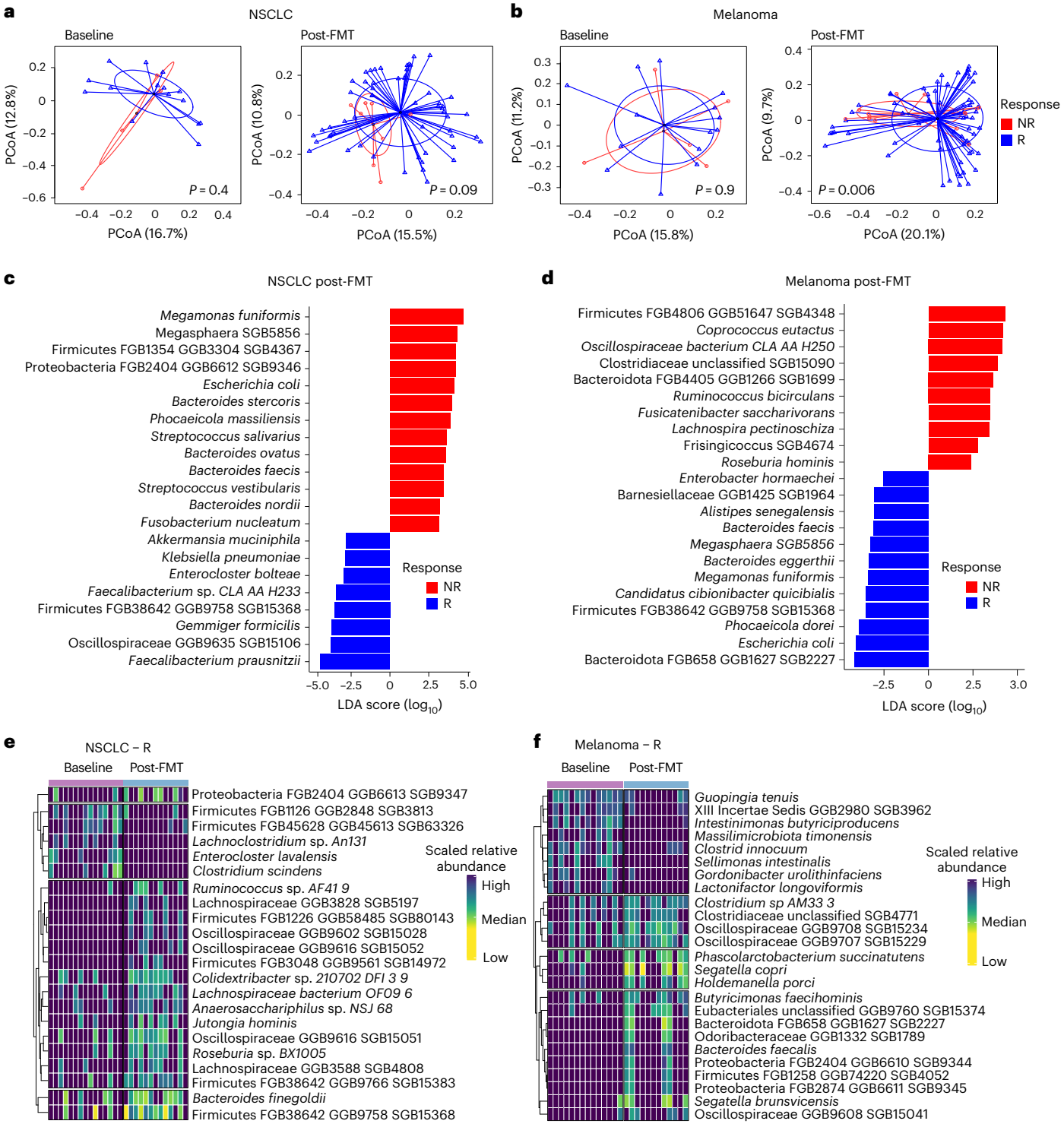

Fig. 3 | Relationship between the gut microbiome and clinical efficacy. **a**–**b**, Principal coordinate analysis (PCoA) representing β-diversity of baseline versus post-FMT samples in NSCLC ($n = 84$ samples from $n = 19$ patients; **a**) and in melanoma ($n = 98$ samples from $n = 20$ patients; **b**). Group differences in dispersion were assessed and measured using β-diversity dispersion. **c**–**d**, LDA using LEfSe representation in NSCLC ($n = 65$ samples from $n = 19$ patients; **c**) and melanoma ($n = 79$ samples from $n = 20$ patients; **d**) after FMT comparing R to NR. Significant values had LDA scores greater than 2 and $P < 0.05$. **e**–**f**, Heatmap representation comparing responders at baseline compared to 1 month after FMT in NSCLC ($n = 28$ samples from $n = 15$ patients; **e**) and melanoma ($n = 26$ samples from $n = 14$ patients; **f**). Bacteria with $P < 0.05$ according to Wilcoxon test between timepoints are shown in the heatmaps.

($P = 0.011$) and melanoma ($P = 0.096$) subgroups (Fig. 4d). In accordance with the lack of differences in α-diversity (Extended Data Fig. 4b), we did not observe any significant decrease in overall SGBs counts in R patients over time after FMT (Extended Data Fig. 5b). This stability of overall SGBs count over time in R patients was explained by an acquisition of SGBs from the donor (category 1) or new SGBs (category 5) (Extended Data Fig. 5b). We confirmed that overall biomass did not change in R patients or in those with high median SGBs loss over time by performing quantitative polymerase chain reaction (qPCR) of the 16S rRNA gene (Extended Data Fig. 5c,d).

The top SGBs lost in R patients included canonically harmful taxa associated with ICI resistance[14,30,31], including *Enterocloster citroniae*, *Enterocloster bolteae*, *C. innocuum*, *Clostridium saudiense*, *Clostridium spiroforme*, *Ruminococcus gnavus* (now a member of *Mediterraneibacter* genus), *Dialister invisus* and *Sellimonas intestinalis* (Fig. 4e and Extended Data Fig. 5e,f). Although *Akkermansia muciniphila* was one of the most frequently depleted species in NSCLC R, patients with aberrantly high relative abundances of *A. muciniphila* exceeding the 77th percentile (associated with dysbiosis[31,35]) experienced elimination of this species (Extended Data Fig. 5g). Examining the impact of the donor on on the degree of SGBs lost, we observed heterogeneity among individual donors (Extended Data Fig. 5h), with a trend for more pronounced SGB loss in cluster B ($P = 0.07$) (Extended Data Fig. 5i).

We next sought to validate our metagenomics findings using orthogonal approaches. We employed a validated qPCR-based assay of 108 selected species[30,38] and confirmed that qPCR relative abundances significantly correlated with shotgun metagenomic data (Extended Data Fig. 6a). This qPCR-based approach—which, unlike metagenomics, is not limited by sequencing depth—demonstrated that the magnitude of species lost relative to the patient's baseline significantly correlated with the corresponding losses detected by metagenomics ($P < 0.001$) (Fig. 4g). Moreover, using this qPCR assay, loss of species from the patient's baseline was also associated with response ($P = 0.012$) (Extended Data Fig. 6b). To further strengthen this observation that loss of baseline SGBs was more strongly associated with response than the acquisition of donor-derived SGBs, we performed high-throughput culturomics in four R patients at baseline and at 1 month after FMT. At baseline, we isolated a mean of 54 species, spanning a total of 217 strains, compared to after FMT with a mean of 45 species, spanning a total of 183 strains ($P = 0.171$) (Extended Data Fig. 6c). As observed in the metagenomics results, we confirmed that significantly more species were lost in these R patients after FMT—defined as species detected in the sample at baseline but no longer detected in the post-FMT sample by culturomics—compared to those engrafted from their respective donors ($P = 0.029$) (Fig. 4h). Similar to the metagenomics results, the lost species in R patients belonged to genera that are considered as harmful, such as *Enterocloster*, *Streptococcus* and *Dialister* (Extended Data Fig. 6d).

We then processed publicly available metagenomic data from published FMT trials and applied our SGB loss pipeline to these data. We observed similar results with regards to elimination of baseline SGBs associated with R patients in our previously published phase 1 trial (MIMIC)[23] of FMT in combination with anti-PD-1 in patients with untreated melanoma ($P = 0.018$) (Extended Data Fig. 7a) and in the first two published studies of FMT in combination with anti-PD-1 in refractory melanoma ($P = 0.074$ for Baruch et al.[21] and $P = 0.002$ for Davar et al.[20]) (Extended Data Fig. 7b,c). Accordingly, pooling these results together validated the conclusion that loss of baseline SGBs was associated with favorable clinical responses ($P < 0.001$) (Fig. 4f). Consistent results were obtained when reanalyzing the metagenomic data from our study as well as all published studies using an independent metagenomics pipeline (BiomScope), whereby NR patients exhibited higher retention of their baseline species (Extended Data Fig. 7d). Taken together, these findings suggest that microbiome remodeling by depletion of pre-existing species may be more critical to therapeutic response than engraftment of specific donor-derived species.

Finally, to validate the relevance of lost bacterial species observed in patients, we performed FMT in antibiotic-treated specific pathogen-free (SPF) conditions[8,39] (Fig. 4i). We recolonized antibiotic-pretreated mice with stool sourced from two R patients with NSCLC after FMT as previously performed[23]. To assess the functional relevance of specific bacterial losses after FMT, we reintroduced a cocktail of bacteria isolated from the baseline sample that were depleted after FMT, specifically, for R1 (*Streptococcus mutans*, *C. innocuum*, *Streptococcus parasanguinis* and *Enterocloster lavalensis*) and for R2 (*Enterocloster clostridioformis*, *Streptococcus anginosus* and *Clostridium tertium*) into FMT-recipient mice by gavage. Activity of anti-PD-1 with or without anti-CTLA-4 was inhibited in the groups of mice receiving FMT plus the cocktails compared to controls receiving R FMT alone ($P = 0.028$ for anti-PD-1 alone and $P = 0.022$ for anti-PD-1 combined with anti-CTLA-4), suggesting that the loss of deleterious species is necessary to achieve the full therapeutic benefit of FMT when combined with ICI (Fig. 4j and Extended Data Fig. 7e,f).

Bacterial loss shapes metabolic and immune landscape

Our results suggest that the response to FMT may be better explained by the loss of a group of deleterious bacteria rather than solely by the engraftment of individual donor strains. To investigate how bacterial loss affects the function of the global microbiome composition, we conducted untargeted plasma metabolomics to assess systemic changes in the metabolic profile after FMT. Across all cohorts, NR patients showed a significant within-group time effect for increased levels of quinolinic acid and kynurenine ($P < 0.001$) (Fig. 5a). Both quinolinic acid and kynurenine are metabolites of the tryptophan pathway and have been causatively linked to resistance to ICI[40–42]. In line with the notion that absence of bacterial loss was associated with resistance to therapy in our study, patients with low proportion of bacterial loss relative to their baseline had higher concentrations of plasma tryptophan after FMT ($P = 0.004$) (Extended Data Fig. 8a). Next, examining the metabolomic profile in the feces, we found that metabolism of the tryptophan pathway significantly decreased over time in R patients, and distinct species contributed to these tryptophan pathway dynamics in NSCLC compared to melanoma, consistent with cohort-specific bacterial signatures affecting responders in each malignancy (Fig. 5b). Taken together, these results suggest functional redundancy across different taxa in both the plasma and feces, with convergence of effects on the tryptophan pathway distinguishing R patients from NR patients after FMT.

Fig. 4 | Association between loss of baseline bacteria and clinical efficacy. **a**–**b**, Representative bar plot of absolute number of SGBs from one NR (**a**) and one R (**b**) patient with melanoma. **c**–**d**, Absolute loss in SGBs after FMT according to response status for FMT-LUMINate NSCLC and melanoma ($n = 122$ samples from $n = 32$ patients) (two-sided) (**c**) and for NSCLC ($n = 54$ samples from $n = 15$ patients) and melanoma ($n = 68$ samples from $n = 17$ patients), *P* value computed by Wilcoxon test (two-sided) (**d**), subgroups. Patients with matching metagenomics form the donors included in this analysis. **e**, Top 50 lost SGBs after FMT in responders for NSCLC and melanoma. **f**, Pooled analysis of post-FMT samples according to response in FMT-LUMINate, MIMIC, ref. 20 and ref. 21 ($P = 1.8 \times 10^{-14}$) ($n = 352$ samples from $n = 69$ patients); *P* value computed by ANOVA test (two-sided). **g**, Spearman's *r* correlation (two-sided) between total SGBs lost, as determined by metagenomics and total species lost, as determined by qPCR ($P < 0.0001$; $n = 104$ samples from $n = 28$ patients). **h**, Culturomics analysis of four patients pre-FMT and post-FMT and comparison of species engrafted from the donor (using the corresponding metagenomics donor sample) compared to species lost after FMT; *P* value computed by non-parametric Mann–Whitney *U*-test (two-sided). **i**, Experimental setting: post-FMT sample from R with NSCLC orally transferred in antibiotic-treated SPF mice. Two weeks later, MCA-205 sarcoma cells were inoculated, and anti-PD-1 or anti-PD-1 plus anti-CTLA-4 was injected intraperitoneally every 3 days. As of day 3, mice also received oral gavage with bacterial cocktail or NaCl every 3 days. **j**, Tumor measurements at euthanization for $n = 10$ mice per group, results from three independent experiments using two different R samples and two different cocktails; *P* values were calculated using Mann–Whitney–Wilcoxon test (two-tailed). Mean ± s.e.m. is represented. For box plots, the center line represents the median, box bounds represent the interquartile range (IQR), whiskers extend to 1.5 × IQR and each dot represents an individual patient sample. 1m, 1 month; 1w, 1 week; 2m, 2 months; αPD1, anti-PD-1; αCTLA4, anti-CTLA-4; ATB, antibiotics; D, day; WT, wild-type.

https://doi.org/10.1038/s41591-025-04186-5

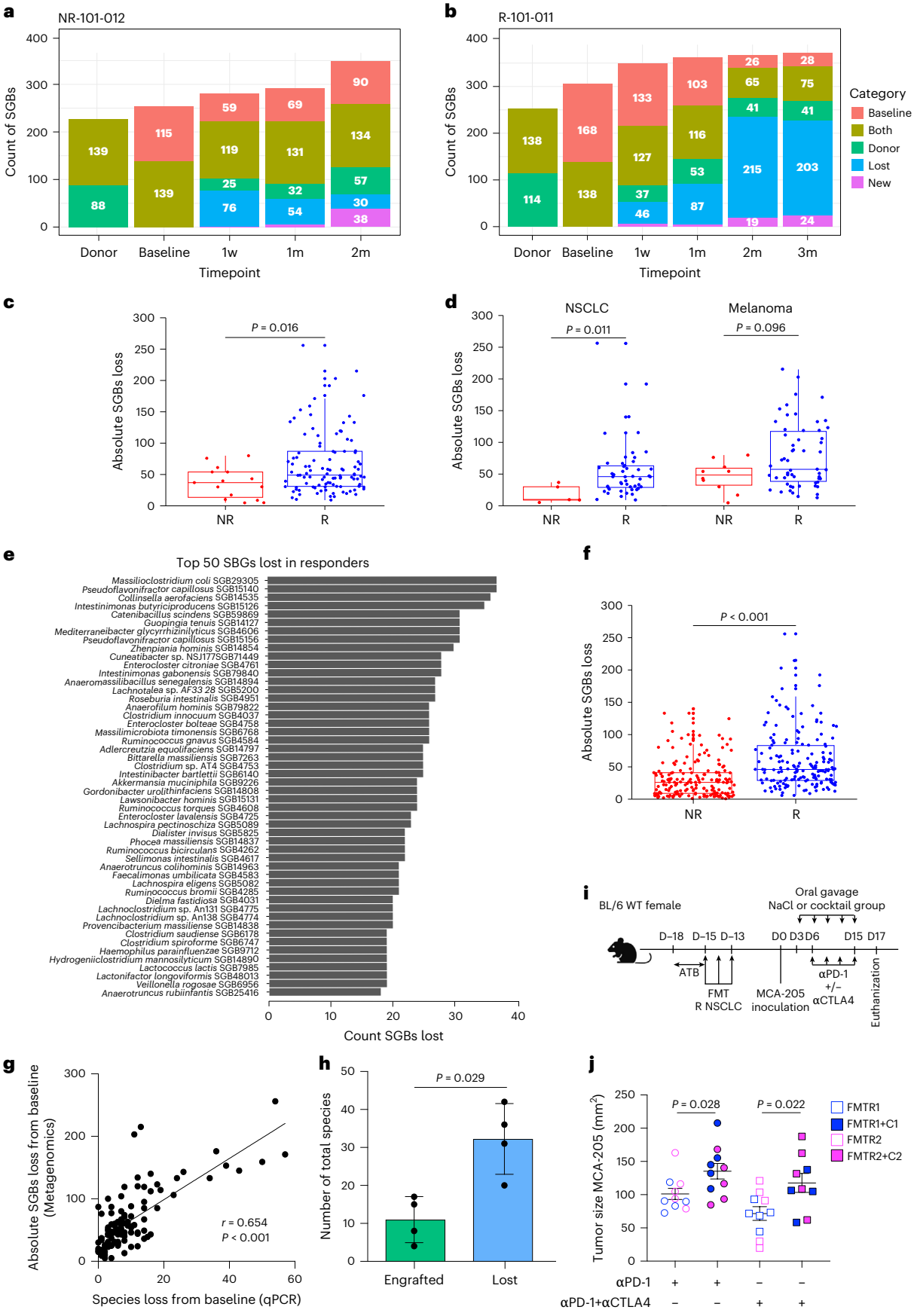

In addition to the metabolomic profile, we examined the impact of bacterial loss on circulating inflammatory markers using high-throughput proteomics. Patients with high proportion of bacterial loss relative to their baseline exhibited distinct clustering of systemic circulating inflammatory proteins after FMT ($P = 0.001$) as opposed to patients with low bacterial loss, where no distinct clustering was observed (Extended Data Fig. 8b). Patients with high bacterial loss exhibited significant increase in distinct circulating pro-inflammatory proteins after FMT, including IFNγ, CXCL9, CXCL13, CCL20, CD8A, CD4 and CD28, whereas patients with low bacterial loss exhibited no distinct changes in circulating proteins after FMT (Extended Data Fig. 8c). We next investigated the impact of bacterial loss on the metabolic profile and on systemic immunity. Patients with pronounced bacterial loss exhibited an increase in the frequency of circulating $CD69^{+}CD8^{+}$ T cells (Fig. 5c) (see Extended Data Fig. 9 for the gating strategies and Supplementary Fig. 3a for this subset in R versus NR after FMT) but a decrease in circulating $CD127^{low}CD25^{high}CD4^{+}$ regulatory T cells (Fig. 5d). Linking these findings with the metabolic profile, high plasma concentrations of quinolinic acid were associated with a reduced frequency of circulating $CD8^{+}$ lymphocyte subpopulations, including $PD\text{-}1^{+}CD8^{+}$ T cells (Fig. 5e and Supplementary Fig. 3b, showing this subset in R versus NR after FMT) and $PD\text{-}1^{+}CD45RA^{-}CCR7^{-}$ effector memory $CD8^{+}$ T cells (Fig. 5f and Supplementary Fig. 3c, showing this subset in R versus NR after FMT). High quinolinic acid was also associated with an increased frequency of circulating $CD127^{low}CD25^{high}CD4^{+}$ effector memory regulatory T cells (Fig. 5g). Taken together, these results suggest that failure to eliminate baseline deleterious taxa may sustain an immunosuppressive metabolic and systemic immune milieu that compromises ICI responses.

Discussion

Our study demonstrates that FMT from healthy donors can enhance the clinical activity of ICI in two malignant diseases treated with two different ICI backbones. In patients with treatment-naive NSCLC and high PD-L1 expression, FMT prior to anti-PD-1 monotherapy resulted in an ORR that exceeded the prespecified efficacy threshold, meeting the primary endpoint in our study. In addition, the ORR of 80% observed in NSCLC was higher than previously described historical data, which range from 39% to 46%[1,3,43]. In the melanoma cohort, administration of FMT before combination nivolumab and ipilimumab similarly yielded an ORR of 75%, exceeding the historical expected response rate of ipilimumab and nivolumab of 50–58%[44]. This supports the potential of FMT to overcome primary resistance to ICI and will be assessed as part of the CanBiome2 (NCT06623461) randomized trial evaluating FMT (LND-101) in combination with ICI in 128 patients.

FMT was well tolerated in combination with anti-PD-1 in patients with NSCLC, with no grade 3 or higher AEs, whereas, in historical cohorts, single-agent pembrolizumab led to grade 3 or higher AEs in approximately 10% of patients[1]. However, in the melanoma cohort receiving dual ICI therapy, we observed a potentially accelerated onset of immune-related AEs and also a higher-than-expected frequency of myocarditis at 15%, which has an incidence of less than 1% in the literature[45]. In addition, the median onset of severe toxicity was 40 days, compared to 60 days in the literature[26]. These toxicities clustered in recipients of FMT donors enriched in *Prevotella* spp. and were not observed in patients receiving anti-PD-1 monotherapy (this donor provided FMT seven times in the MIMIC trial in combination with anti-PD-1 monotherapy and once in the NSCLC cohort also receiving anti-PD-1 monotherapy, and none of these patients experienced grade 3 or higher AEs). These findings suggest a context-dependent interaction between specific microbial taxa and ICI backbone and implicate *Prevotella* spp. as a potential driver of AEs in the setting of dual immune checkpoint blockade targeting both PD-1 and CTLA-4. As such, myocarditis has been designated an AE of special interest in the ongoing randomized CanBiome2 trial (NCT06623461), where this safety signal will be prospectively monitored. In addition, donor 5 has been excluded from participating in future FMT trials. Our study highlights the importance of donor selection for future trials.

Mechanistically, our results suggest that clinical benefit from FMT is not mediated by the number of specific donor-derived strains. Although certain taxa, including *F. prausnitzii*, were enriched in some R patients, these associations lacked overlap across cohorts. In addition, strain-level engraftment did not differ between R and NR patients across our study and in multiple published studies[23]. By contrast, clinical responses were associated with a robust pattern of depletion of several deleterious bacterial species, including SIG1 (ref. 30), present at baseline from the *Clostridium*, *Enterocloster*, *Streptococcus* and *Dialister* genera. This pattern of bacterial loss was validated by metagenomics, qPCR and high-throughput culturomics. It is important to note that the two latter techniques are not limited by sequencing depth. Moreover, this pattern of microbial depletion was corroborated in three published FMT trials[20,21,23] and also in the concurrent TACITO trial[46], underscoring its general validity across different geographies (Asia, Europe and North America), pathologies and treatment regimens. Notably, the TACITO trial demonstrated a significant improvement in median PFS, and elimination of baseline species was noted only in the FMT group and not in the placebo group. In our study, when reintroduced into tumor-bearing mice after oral gavage of favorable FMT, these harmful bacteria led to anti-PD-1 resistance. These findings suggest that therapeutic response of FMT may result from the elimination of immunosuppressive pathobionts. In line with this speculation, we detected consistent signals at the functional level, with relative depletion of the immunosuppressive tryptophan pathway and specific tryptophan metabolites, particularly kynurenine and quinolinic acid, among R patients after FMT. Of note, serum tryptophan has been associated with poor prognosis in patients with cancer[47]. Mechanistically, tryptophan metabolism has been found to activate the aryl hydrocarbon receptor (AHR) to promote immune suppression in the tumor microenvironment[48–50]. In our study, high bacterial loss was associated with a favorable immunometabolic profile—characterized by increased effector $CD8^{+}$ T cells, decreased regulatory T cells and reduced tryptophan metabolism.

Fig. 5 | Metabolic and immune profiling after FMT according to clinical efficacy. a, Longitudinal plasma analysis of quinolinic acid (top) and kynurenine (bottom) metabolites measured by UHPLC–MS; for each metabolite, two representations are shown: smooth trajectories of the model-predicted mean intensity for R (blue) and NR (red) over time. Shaded bands represent 95% confidence intervals around the fitted mean; *P* values indicate statistical significance of each smooth term. Right: pointwise differences between the predicted mean of the two groups (R − NR) with 95% confidence intervals (gray shaded area). Pink horizontal segments indicate time periods where confidence intervals exclude zero, representing significant between-group differences. Data were fitted using generalized additive mixed models with Tweedie distribution and random subject intercepts ($n = 100$ samples from $n = 35$ patients; Methods). **b**, MetaCyc representation of the tryptophan pathway comparing baseline to after FMT in NSCLC R ($n = 62$ samples from $n = 15$ patients) and melanoma R ($n = 71$ samples from $n = 15$ patients); *P* values were computed by the Wald test (two-sided) from DESeq2 analysis. **c**–**d**, Spearman's *r* correlation (two-sided) of flow cytometry analysis from NSCLC and melanoma patient PBMCs after FMT according to low versus high median SGB loss from baseline for frequency of $CD69^{+}CD8^{+}$ T cells (**c**) and $CD127^{low}CD25^{high}CD4^{+}$ regulatory T cells (**d**). Spearman's *r* correlation (two-sided) of flow cytometry analysis from NSCLC and melanoma patient PBMCs after FMT according to low versus high plasma quinolinic acid for $PD\text{-}1^{+}CD8^{+}$ T cells (**e**), $PD\text{-}1^{+}$ effector memory $CD8^{+}$ T cells (**f**) and effector memory regulatory T cells (**g**) from $n = 50$ samples. Abs $\log_2$FC, absolute $\log_2$ fold change; EM, effector memory; Hi, high; Lo, low; PWY−6629, superpathway of L-tryptophan biosynthesis; T_{reg}, regulatory T; TRPSYN−PWY, L-tryptophan biosynthesis.

https://doi.org/10.1038/s41591-025-04186-5

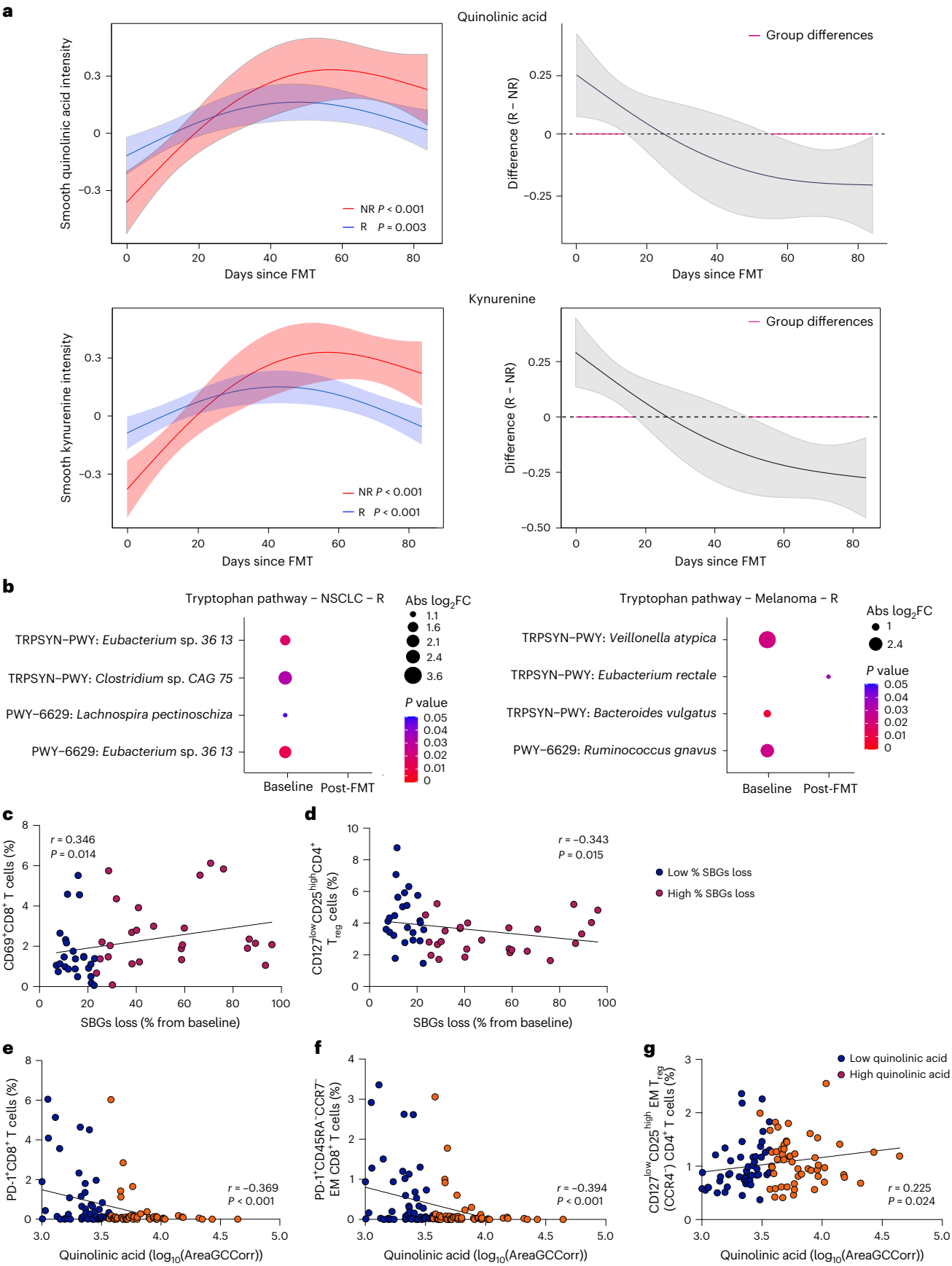

This study has several limitations, including the single-arm design, use of multiple donors and limited power for R/NR comparisons due to the low number of NR patients. In addition, the interplay among toxicity, efficacy and bacterial loss from the intestinal tract must be explored in future mechanistic studies. Nonetheless, our data provide strong evidence in favor of the efficacy of FMT in the context of immune checkpoint inhibition. Our study identified a potentially pharmacodynamic biomarker for FMT efficacy, which is the elimination of deleterious bacteria from the intestinal microbiota. This finding may affect the design of next-generation live biotherapeutic products that should be designed not only to engraft but also to induce the depletion of deleterious pathobionts from the intestinal lumen.

To our knowledge, the FMT-LUMINate phase 2 clinical trial provides the first prospective evidence that FMT from healthy donors can enhance the efficacy of ICI in NSCLC in combination with anti-PD-1 and in melanoma in combination with anti-PD1 plus anti-CTLA-4, demonstrating that FMT efficacy is reproducible across tumor pathologies and ICI backbones. Our findings that *Prevotella* spp. is associated with accelerated toxicity only in the context of anti-CTLA-4 therapy highlight the need to select donors and rationally design future FMT studies according to the ICI backbone. Mechanistically, the therapeutic effect of FMT may be driven by the elimination of deleterious bacteria—most notably *Enterocloster*, *Clostridium* and *Streptococcus* spp.—that were present at baseline. This bacterial depletion was associated with a favorable immunometabolic milieu, including reduction in quinolinic acid and expansion of $CD8^+$ memory T cells. These results offer an actionable framework for donor selection, biomarker development and design of next-generation microbial therapies aimed at selectively eliminating immunosuppressive pathobionts.

Online content

Any methods, additional references, Nature Portfolio reporting summaries, source data, extended data, supplementary information, acknowledgements, peer review information; details of author contributions and competing interests; and statements of data and code availability are available at https://doi.org/10.1038/s41591-025-04186-5.

References

1. Reck, M. et al. Pembrolizumab versus chemotherapy for PD-L1–positive non–small-cell lung cancer. *N. Engl. J. Med.* **375**, 1823–1833 (2016).
2. Wolchok, J. D. et al. Overall survival with combined nivolumab and ipilimumab in advanced melanoma. *N. Engl. J. Med.* **377**, 1345–1356 (2017).
3. Mok, T. S. K. et al. Pembrolizumab versus chemotherapy for previously untreated, PD-L1-expressing, locally advanced or metastatic non-small-cell lung cancer (KEYNOTE-042): a randomised, open-label, controlled, phase 3 trial. *Lancet* **393**, 1819–1830 (2019).
4. Elkrief, A. et al. Efficacy of PD-(L)1 blockade monotherapy compared with PD-(L)1 blockade plus chemotherapy in first-line PD-L1-positive advanced lung adenocarcinomas: a cohort study. *J. Immunother. Cancer* **11**, e006994 (2023).
5. Sharma, P., Hu-Lieskovan, S., Wargo, J. A. & Ribas, A. Primary, adaptive, and acquired resistance to cancer immunotherapy. *Cell* **168**, 707–723 (2017).
6. Sivan, A. et al. Commensal *Bifidobacterium* promotes antitumor immunity and facilitates anti-PD-L1 efficacy. *Science* **350**, 1084–1089 (2015).
7. Vétizou, M. et al. Anticancer immunotherapy by CTLA-4 blockade relies on the gut microbiota. *Science* **350**, 1079–1084 (2015).
8. Routy, B. et al. Gut microbiome influences efficacy of PD-1–based immunotherapy against epithelial tumors. *Science* **359**, 91–97 (2018).
9. Gopalakrishnan, V. et al. Gut microbiome modulates response to anti–PD-1 immunotherapy in melanoma patients. *Science* **359**, 97–103 (2018).
10. Matson, V. et al. The commensal microbiome is associated with anti–PD-1 efficacy in metastatic melanoma patients. *Science* **359**, 104–108 (2018).
11. Hanahan, D. Hallmarks of cancer: new dimensions. *Cancer Discov.* **12**, 31–46 (2022).
12. Elkrief, A. et al. The gut microbiome as a target in cancer immunotherapy: opportunities and challenges for drug development. *Nat. Rev. Drug Discov.* **24**, 685–704 (2025).
13. Derosa, L. et al. Gut bacteria composition drives primary resistance to cancer immunotherapy in renal cell carcinoma patients. *Eur. Urol.* **78**, 195–206 (2020).
14. Thomas, A. M. et al. Gut OncoMicrobiome Signatures (GOMS) as next-generation biomarkers for cancer immunotherapy. *Nat. Rev. Clin. Oncol.* **20**, 583–603 (2023).
15. Fidelle, M. et al. A microbiota-modulated checkpoint directs immunosuppressive intestinal T cells into cancers. *Science* **380**, eabo2296 (2023).
16. Elkrief, A. et al. Antibiotics are associated with worse outcomes in lung cancer patients treated with chemotherapy and immunotherapy. *npj Precis. Oncol.* **8**, 143 (2024).
17. Elkrief, A. et al. The negative impact of antibiotics on outcomes in cancer patients treated with immunotherapy: a new independent prognostic factor? *Ann. Oncol.* **30**, 1572–1579 (2019).
18. Elkrief, A. et al. Gut microbiota in immuno-oncology: a practical guide for medical oncologists with a focus on antibiotics stewardship. *Am. Soc. Clin. Oncol. Educ. Book* **45**, e472902 (2025).
19. Hakozaki, T. et al. The gut microbiome associates with immune checkpoint inhibition outcomes in patients with advanced non-small cell lung cancer. *Cancer Immunol. Res.* **8**, 1243–1250 (2020).
20. Davar, D. et al. Fecal microbiota transplant overcomes resistance to anti-PD-1 therapy in melanoma patients. *Science* **371**, 595–602 (2021).
21. Baruch, E. N. et al. Fecal microbiota transplant promotes response in immunotherapy-refractory melanoma patients. *Science* **371**, 602–609 (2021).
22. Elkrief, A. & Routy, B. First clinical proof-of-concept that FMT can overcome resistance to ICIs. *Nat. Rev. Clin. Oncol.* **18**, 325–326 (2021).
23. Routy, B. et al. Fecal microbiota transplantation plus anti-PD-1 immunotherapy in advanced melanoma: a phase I trial. *Nat. Med.* **29**, 2121–2132 (2023).
24. Seo, Y. D., Ajami, N. & Wargo, J. A. Using gut microorganisms to treat cancer. *Nat. Med.* **29**, 1910–1911 (2023).
25. Bray, J. R. & Curtis, J. T. An ordination of the upland forest communities of southern Wisconsin. *Ecol. Monogr.* **27**, 325–349 (1957).
26. Schneider, B. J. et al. Management of immune-related adverse events in patients treated with immune checkpoint inhibitor therapy: ASCO guideline update. *J. Clin. Oncol.* **39**, 4073–4126 (2021).
27. Shannon, C. E. A mathematical theory of communication. *Bell Syst. Tech. J.* **27**, 379–423 (1948).
28. Anderson, M. J., Ellingsen, K. E. & McArdle, B. H. Multivariate dispersion as a measure of beta diversity. *Ecol. Lett.* **9**, 683–693 (2006).
29. Blanco-Miguez, A. et al. Extending and improving metagenomic taxonomic profiling with uncharacterized species with MetaPhlAn 4. *Nat. Biotechnol.* https://doi.org/10.1038/s41587-023-01688-w (2022).
30. Derosa, L. et al. Custom scoring based on ecological topology of gut microbiota associated with cancer immunotherapy outcome. *Cell* **187**, 3373–3389 (2024).

31. Birebent, R. et al. Surrogate markers of intestinal dysfunction associated with survival in advanced cancers. *Oncoimmunology* **14**, 2484880 (2025).
32. Goel, A. et al. Toward a health-associated core keystone index for the human gut microbiome. *Cell Rep.* **44**, 115378 (2025).
33. Yonekura, S. et al. Cancer induces a stress ileopathy depending on β-adrenergic receptors and promoting dysbiosis that contributes to carcinogenesis. *Cancer Discov.* **12**, 1128–1151 (2022).
34. Gacesa, R. et al. Environmental factors shaping the gut microbiome in a Dutch population. *Nature* **604**, 732–739 (2022).
35. Derosa, L. et al. Intestinal *Akkermansia muciniphila* predicts clinical response to PD-1 blockade in patients with advanced non-small-cell lung cancer. *Nat. Med.* **28**, 315–324 (2022).
36. Gopalakrishnan, V. et al. Gut microbiome modulates response to anti-PD-1 immunotherapy in melanoma patients. *Science* **359**, 97–103 (2018).
37. Pasolli, E. et al. Extensive unexplored human microbiome diversity revealed by over 150,000 genomes from metagenomes spanning age, geography, and lifestyle. *Cell* **176**, 649–662 (2019).
38. Messaoudene, M. et al. The DAV132 colon-targeted adsorbent does not interfere with plasma concentrations of antibiotics but prevents antibiotic-related dysbiosis: a randomized phase I trial in healthy volunteers. *Nat. Commun.* **15**, 8083 (2024).
39. Messaoudene, M. et al. A natural polyphenol exerts antitumor activity and circumvents anti-PD-1 resistance through effects on the gut microbiota. *Cancer Discov.* **12**, 1070–1087 (2022).
40. Maria Rain, J., David, M. & John, B. Immunosuppressive metabolites in tumoral immune evasion: redundancies, clinical efforts, and pathways forward. *J. Immunother. Cancer* **9**, e003013 (2021).
41. Moffett, J. R. & Namboodiri, M. A. Tryptophan and the immune response. *Immunol. Cell Biol.* **81**, 247–265 (2003).
42. Kesarwani, P. et al. Quinolinate promotes macrophage-induced immune tolerance in glioblastoma through the NMDAR/PPARγ signaling axis. *Nat. Commun.* **14**, 1459 (2023).
43. Larkin, J. et al. Five-year survival with combined nivolumab and ipilimumab in advanced melanoma. *N. Engl. J. Med.* **381**, 1535–1546 (2019).
44. Larkin, J. et al. Combined nivolumab and ipilimumab or monotherapy in untreated melanoma. *N. Engl. J. Med.* **373**, 23–34 (2015).
45. Ozaki, A. F. et al. Incidence and survival outcomes of myocarditis and pericardial diseases associated with immune checkpoint inhibitor therapy. *Cardiooncology* **11**, 26 (2025).
46. Porcari, S. et al. Fecal microbiota transplantation plus pembrolizumab and axitinib in metastatic renal cell carcinoma: the randomized phase 2 TACITO trial. *Nat. Med.* https://doi.org/10.1038/s41591-025-04189-2 (2026).
47. Alves Costa Silva, C. et al. Influence of microbiota-associated metabolic reprogramming on clinical outcome in patients with melanoma from the randomized adjuvant dendritic cell-based MIND-DC trial. *Nat. Commun.* **15**, 1633 (2024).
48. Schramme, F. et al. Inhibition of tryptophan-dioxygenase activity increases the antitumor efficacy of immune checkpoint inhibitors. *Cancer Immunol. Res.* **8**, 32–45 (2020).
49. Liu, Y. et al. Tumor-repopulating cells induce PD-1 expression in $CD8^+$ T cells by transferring kynurenine and AhR activation. *Cancer Cell* **33**, 480–494 (2018).
50. Trefny, M. P., Kroemer, G., Zitvogel, L. & Kobold, S. Metabolites as agents and targets for cancer immunotherapy. *Nat. Rev. Drug Discov.* **24**, 764–784 (2025).

Sreya Duttagupta[1,2,24], Meriem Messaoudene[1,24], Sebastian Hunter[1], Antoine Desilets[1,3], Rahima Jamal[1,3], Catalin Mihalcioiu[4], Wiam Belkaid[1], Nicolas Marcoux[5], Marine Fidelle[6], Deborah Suissa[6], Mayra Ponce[1], Mallia Geiger[1], Julie Malo[1], Gianmarco Piccinno[7], Michal Punčochář[7], Alysé Filin[1], Vitor Heidrich[7], Diana Rusu[1], Babacar Mbaye[1], Sylvere Durand[8,9], Imen Ben Aissa[1], Vadim Puller[10], Raynald de Lahondès[10], Normand Blais[1,3], Mustapha Tehfe[1,3], Scott Owen[4], Karl Bélanger[1,3], Seema Nair Parvathy[11,12,13], Benjamin Shieh[4], Jacques Raphael[14,15], John Lenehan[14,15], Daniel Breadner[14,15], Jeffrey Rothenstein[16], Nicholas Rozza[4], Jade Maillou[1,2], Somayeh Nili[1], Diogjena Katerina Prifti[1], Federica Pinto[7], Federica Armanini[7], Seunghee Kim-Schulze[17], Thomas U. Marron[17], Guido Kroemer[8,9,18,19], Lisa Derosa[6,20], Laurence Zitvogel[6,20], Michael Silverman[11,12,13], Nicola Segata[7], Saman Maleki Vareki[14,21,22,23], Bertrand Routy[1,3,25] & Arielle Elkrief[1,3,25] ✉

[1]Axe Cancer, Centre de recherche du Centre hospitalier de l'Université de Montréal (CRCHUM), Montréal, Québec, Canada. [2]Department of Microbiology & Immunology, Faculty of Medicine, Université de Montréal, Montréal, Québec, Canada. [3]Hemato-Oncology Division, Centre hospitalier de l'Université de Montréal (CHUM), Montréal, Québec, Canada. [4]Departments of Oncology and Medicine, McGill University, Montreal, Québec, Canada. [5]Hemato-Oncology Division, Centre hospitalier de l'Université de Québec, Québec City, Québec, Canada. [6]Université Paris-Saclay, U1015 INSERM, Gustave Roussy, Ligue Labellisée contre le Cancer, Villejuif, France. [7]Department of Computational, Cellular and Integrative Biology, University of Trento, Trento, Italy. [8]Centre de Recherche des Cordeliers, Équipe labellisée par la Ligue contre le cancer, Institut Universitaire de France, Paris, France. [9]Université Paris-Saclay, INSERM US23 / CNRS UAR 3655, Metabolomics and Cell Biology Platforms, Institut Gustave Roussy, Villejuif, France. [10]GMT Science, Rouen, France. [11]Department of Medicine, Division of Infectious Diseases, Western University, London, Ontario, Canada. [12]Division of Infectious Diseases, St. Joseph's Health Care, London, Ontario, Canada. [13]Lawson Research Institute, London, Ontario, Canada. [14]Verspeeten Family Cancer Centre at London Health Sciences Centre, London, Ontario, Canada. [15]Department of Oncology, Division of Medical Oncology, Schulich School of Medicine

and Dentistry at Western University, London, Ontario, Canada. [16]R.S. McLaughlin Durham Regional Cancer Center at Lakeridge Health, Oshawa, Ontario, Canada. [17]Tisch Cancer Center, Icahn School of Medicine at Mount Sinai, New York, NY, USA. [18]Université Paris Cité, Sorbonne Université, Inserm, Centre de Recherche des Cordeliers, Paris, France. [19]Institut du Cancer Paris CARPEM, Department of Biology, Hôpital Européen Georges Pompidou, AP-HP, Paris, France. [20]Gustave Roussy Cancer Campus (GRCC), ClinicObiome, Villejuif, France. [21]Department of Pathology and Laboratory Medicine, Western University, London, Ontario, Canada. [22]Division of Experimental Oncology, Department of Oncology, Western University, London, Ontario, Canada. [23]Ontario Institute of Cancer Research, Toronto, Ontario, Canada. [24]These authors contributed equally: Sreya Duttagupta, Meriem Messaoudene. [25]These authors jointly supervised this work: Bertrand Routy, Arielle Elkrief. ✉e-mail: arielle.elkrief@umontreal.ca

Methods

Study participants and clinical trial design

The FMT-LUMINate trial (NCT04951583) is a multicenter, open-label, phase 2 trial that included patients with advanced NSCLC, cutaneous melanoma and uveal melanoma who were being treated with first-line ICI therapy. Biological sex was considered in the study based on self-report. Gender was not considered in the study. Patients were 18 years of age or older with histologically confirmed diagnosis of NSCLC, cutaneous melanoma or uveal melanoma and measurable disease as per Response Evaluation Criteria in Solid Tumors version 1.1 (RECIST v1.1). An Eastern Cooperative Oncology Group (ECOG) score of 0–2 was required. Previous treatment with palliative surgery or radiation was allowed. For the melanoma cohort, previous adjuvant anti-PD-1 was allowed provided the last dose occurred more than 6 months prior to enrollment. For the melanoma cohort, previous treatment with BRAF/MEK inhibitors was allowed. Major exclusion criteria included previous treatment with anti-PD-1 in the NSCLC cohort, a history of autoimmune diseases, active bowel disease, the use of daily corticosteroids >10 mg of prednisone or equivalent, symptomatic brain metastases or leptomeningeal disease. Patients were enrolled and treated at five academic centers in Canada: the Centre hopitalier de l'Université de Montréal (CHUM; Québec), the London Regional Cancer Program (LRCP; Ontario), the Centre hospitalier de l'Université de Québec (CHUQ; Québec), McGill University Health Centre (MUHC; Québec) and Lakeridge Health (Oshawa, Ontario). The research ethics board at each institution approved the conduct of the trial in accordance with current federal regulations, including the Canadian Food and Drug Regulations (C.05.001); the US Code of Federal Regulations (21 CFR Part 56); International Conference on Harmonization of Technical Requirements for Registration of Pharmaceuticals for Human Use Good Clinical Practice Guidelines; and the Declaration of Helsinki. The Unité d'Innovations Thérapeutiques at the CHUM was responsible for administrative functions, including the establishment of a DSMB, which provided safety oversight for the trial. Trial monitoring of the conduct of the trial and data management were performed by Ozmosis, Inc. All patients provided written informed consent and were able to withdraw consent at any time without compromising their cancer treatment. Patients were not financially compensated for their participation in this study.

Ethics approvals

The clinical trial and correlative analyses were approved by the CHUM Ethics Review Board and each participating center (ethics number MP-02-2022-10121/21.173). For culturomics analysis, this was conducted under project number 2025-12377 through biobank numbers MP-02-2018-7132/17.035 and 16.161.

Patient inclusion and exclusion criteria for enrollment

Inclusion criteria are summarized below:

1. Age 18 years of age or older
2. Confirmed histological diagnosis of advanced cutaneous melanoma, unresectable or advanced uveal melanoma or advanced NSCLC
3. Stage IV or unresectable disease
4. No prior anti-PD1 treatment with the exception of those who received adjuvant therapy (see point 5)
5. For patients with newly diagnosed advance melanoma who relapsed after adjuvant immunotherapy, patients can be included in this study if they relapsed more than 6 months after their last dose of immunotherapy given in the adjuvant setting.
6. For patients with NSCLC, tumor PD-L1 expression level ≥50%
7. Evaluable disease as per immune-related RECIST (iRECIST) or RECIST
8. ECOG performance status of 0–2
9. Ability to ingest capsules
10. Patients receiving systemic steroids at physiologic doses are permitted to enroll provided the dose does not exceed 10 mg prednisone daily or equivalent.
11. Negative pregnancy test for women of childbearing potential
12. Highly effective contraception (any method above 97% success rate) for both male and female patients throughout the study and for at least 60 days after last treatment administration if the risk of conception exists

Exclusion criteria are summarized below:

1. Pregnant or breastfeeding or expecting to conceive or father children within the projected duration of the trial, starting with the prescreening or screening visit through 120 days after the last dose of trial treatment
2. Current or recent (in the last 90 days) long-term exposure to high-dose oral or intravenous corticosteroids
   a. Patients who require intermittent use of bronchodilators, local steroid injections or short-term corticosteroids for any reason including, but not limited to, brain metastases treatment/prophylaxis are permitted to enroll at the discretion of the sponsor.
3. Has a diagnosis of immunodeficiency (for example, HIV and transplantation) or receiving systemic steroid therapy (>10 mg prednisone daily or equivalent) or any other form of active immunosuppressive therapy
4. Presence of a chronic debilitating intestinal disease (for example, malabsorption and colonic tumor)
5. Use of probiotics during FMT. Probiotics must be discontinued a minimum of 24 hours before FMT administration, and patients are not permitted to take probiotics during the course of immunotherapy treatment.
6. Use of antibiotics within 2 weeks of enrollment in the study
7. Presence of absolute contraindications to FMT administration
   a. Toxic megacolon
   b. Severe dietary allergies (for example, shellfish, nuts and seafood)
   c. Active inflammatory bowel disease
8. Expected to require any other form of systemic or localized anti-neoplastic therapy while on study. Palliative radiation therapy is permitted at the discretion of the sponsor.
9. In the last year, has a known history of a malignancy requiring anti-neoplastic treatment:
   a. This time requirement does not apply to patients who underwent successful definitive resection of basal or squamous cell carcinoma of the skin, superficial bladder cancer and in situ cancers, including cervical cancer, breast cancer, melanoma or other in situ cancers.
10. Symptomatic central nervous system metastases
11. Leptomeningeal involvement (leptomeningeal enhancement on magnetic resonance imaging/computed tomography and/or positive cerebrospinal fluid cytology)
12. Has an uncontrolled autoimmune disease that requires active immunosuppressive agents:
    a. Patients with vitiligo, type I diabetes, well-controlled hypothyroidism due to Hashimoto disease or resolved childhood asthma/atopy are not excluded.
13. A history of (non-infectious) pneumonitis that required steroids or current pneumonitis
14. Has serious concomitant illnesses, such as impaired cardiovascular function or clinically significant cardiovascular disease (uncontrolled congestive heart failure requiring treatment (New York Heart Association grade ≥3), uncontrolled hypertension, acute myocardial cardiac ischemia or unstable

angina ≤2 months prior to study entry and severe cardiac arrhythmia) and active inflammatory bowel disorders
15. Has an active infection requiring systemic therapy
16. Patient has received a live vaccine within 4 weeks prior to the first dose of treatment:
    a. Seasonal influenza vaccines for injection are generally inactivated flu vaccines and are allowed; however, intranasal influenza vaccines (for example, Flu-Mist) are live attenuated vaccines and are not allowed.
17. Has known psychiatric or substance abuse disorders that would interfere with cooperation with the requirements of the trial

FMT

Patients underwent a standard bowel preparation with 4,000 ml of PEG3350 liquid solution the evening before a single FMT using oral capsules. FMT capsules (now developed as LND-101) are produced using 80–100 g of feces per dose from screened healthy donors under the supervision of the Division of Infectious Diseases at St. Joseph's Hospital in London, Ontario, Canada. Each dose of capsules contained the feces from a single donor. Major exclusion criteria for healthy donors included any known transmissible pathogen, history of medical illness, any history of major infection, such as COVID-19, monkeypox and hepatitis, and recent travel. A full list of inclusion and exclusion criteria was previously published[23,51]. Donor assignment was performed according to donor availability, without particular selection other than the screening requirements. Patients were required to consume 36–40 capsules under supervision and within 2 hours of defrosting the capsules, followed by a 30-minute period of observation. If a patient required antibiotics for an active infection throughout the study protocol, a 'salvage' FMT was performed within 14 days of the last dose of antibiotics[52]. Salvage FMT was not performed if the treating investigator deemed that the procedure would interfere with patient safety (that is, antibiotics administered during a severe adverse event (SAE) period). Patients were not required to undergo a second bowel preparation in the event of salvage FMT. In the event of *Pneumocystis jirovecii* prophylaxis, salvage FMT was not required.

Donor screening

Donor screening procedures are listed in Appendix 4 of the protocol and as previously published[23].

Capsule preparation

FMT capsules were prepared according to an established protocol as described in our previous study[23]. In brief, feces donations (80–100 g) were processed separately without pooling by mixing in 0.9% normal saline and glycerol and were filtered using a stomacher bag. The filtrate was centrifuged, and the final sediment was mixed to incorporate residual liquid to allow pipetting into capsules as previously published[23].

ICI therapy and assessments

ICI therapy was publicly funded. For the NSCLC cohort, patients received pembrolizumab at 2 mg kg^{-1} every 3 weeks, as per the standard of care. For the melanoma cohort, patients received ipilimumab 3 $mgkg^{-1}$ intravenously plus nivolumab 1 mg kg^{-1} intravenously every 3 weeks for four cycles, followed by maintenance nivolumab 3 mg kg^{-1} every 2 weeks or nivolumab 6 mg kg^{-1} intravenously every 4 weeks. The first cycle of ICI was initiated within 7 days after FMT (Extended Data Fig. 1b). Therapy continued at the discretion of the treating oncologist until unacceptable toxicity, completion of 2 years, progression or death. Routine imaging was completed every 3 months for the first 2 years. Acceptable imaging included computed tomography or magnetic resonance imaging at the discretion of the treating oncologist who was encouraged to use the same modality of imaging throughout whenever possible. The assessment of treatment response was conducted as per RECIST v1.1 (ref. 53) and iRECIST[54] when applicable at 3 months, 6 months and 12 months. Assessment of treatment response at all other timepoints was done by investigator-assessed RECIST. The ORR was defined as the proportion of patients with a complete response or a partial response and designated as 'R' for the translational studies. All other patients (the proportion with stable disease or progressive disease as best response), were designated as 'NR'.

Data and sample collection

At each clinic visit, patient data, to include demographics, clinical and imaging assessments and adverse event recording, were collected per protocol using a secure, password-protected, electronic data capture web-based tool (Medidata Rave Unified Life Science Platform). Patient fecal and blood samples were collected at the following timepoints: before FMT (baseline), the first cycle of ICI therapy (1 week) and the second cycle of ICI therapy (1 month), 2 months, 3 months, 6 months, 9 months and 1 year. A complete clinical assessment was conducted at each visit with routine lab work per standard of care. Patients were permitted to withdraw consent at any time with no impact on treatment, although analysis of previously obtained samples was retained.

Assessment and management of AEs

FMT and ICI-related toxicities were evaluated using the Common Terminology Criteria for Adverse Events version 5.0 (CTCAE v5.0) grading scale[55]. Toxicities were attributed to FMT only if the investigator deemed the AE to be related to FMT and if the AE occurred before the first cycle of ICI. AEs were managed by the treating investigator in accordance with routine clinical practice guidelines. Any patient who experienced an SAE had ICI therapy suspended until resolved or discontinued at the discretion of the treating investigator. All AEs were reviewed by the trial sponsor to ensure consistency in attribution and grading.

Outcomes and sample size

The primary outcome of the study was the ORR in the NSCLC cohort, defined as the proportion of patients whose best objective response was either a complete response or a partial response. Best objective response was determined as the best response recorded from the first dose of study treatment until the last tumor assessment prior to initiation of subsequent therapy.

Secondary outcomes included DCR, defined as the proportion of patients achieving complete response, partial response or stable disease lasting more than 6 months; ORR in the melanoma cohort; and safety of FMT in combination with ICI. Additional secondary outcomes to be reported subsequently include PFS and OS at 12 months in both the NSCLC and cutaneous melanoma cohorts. Microbiome engraftment was evaluated by acquired donor–host similarity using the Bray–Curtis dissimilarity index.

Each cohort was analyzed independently, as outlined in the study protocol, given their differing disease biology and treatment context.

Sample size was determined as follows: for the NSCLC cohort, assuming that the ORR rate is 39% (null hypothesis)[3], a sample size of 18 patients has 80% power to detect an ORR of 64% (alternative hypothesis) using a one-sided binomial test with 0.10 level of significance. Because the prespecified primary endpoint of the study was ORR in the NSCLC cohort, there was no prespecified sample size calculation for the cutaneous melanoma cohort.

The present paper focuses on the NSCLC and cutaneous melanoma cohorts given prespecified primary and secondary endpoints in these groups outlined in the study protocol. Given that the uveal melanoma cohort was explicitly defined to be an exploratory cohort, the uveal melanoma cohort results will be reported separately.

Due to the COVID-19 pandemic and widespread disruptions to clinical trial operations[56–58]—including delayed site activations

and reductions in outpatient oncology services—accrual to the trial was slower than anticipated. The protocol was amended to a total target of 20 patients, enabling evaluation of the primary and key secondary endpoints while maintaining feasibility under pandemic-related constraints.

Metagenomics analysis

Sequencing and processing. A total of 199 fecal samples collected from 39 patients enrolled underwent whole-genome shotgun sequencing. Stool aliquots were preserved at −80 °C in DNA/RNA Shield Buffer (Zymo Research) until processing. DNA extraction was performed using the DNeasy PowerSoil Pro Kit (Qiagen), following the manufacturer's protocol. Sequencing libraries were prepared using the Illumina DNA Prep (M) Tagmentation Kit (Illumina), following the manufacturer's instructions, and purified with a 0.7× ratio of Agencourt AMPure XP beads. Sequencing was conducted on a NovaSeq 6000 S4 flow cell (Illumina) at the University of Trento's in-house sequencing facility (Trento, Italy). Raw reads were processed through a quality control pipeline available at https://github.com/SegataLab/preprocessing. In brief, reads were filtered out if they had low quality ($Q < 20$), were shorter than 75 bp or contained two or more ambiguous bases. Host-derived reads (human genome hg19 and Illumina spike-in phiX174) were also removed. On average, each sample yielded approximately 48 million high-quality reads. Five samples failed internal quality control and were excluded from downstream analyses. Taxonomic profiling was carried out using MetaPhlAn 4 (database version vJun23_CHOCOPhlAnSGB_202307). Of the 194 samples that passed quality control, 12 were excluded from the downstream analysis: 10 of excluded samples occurred during unscheduled visits, and two excluded samples were collected after salvage FMT. Because the salvage FMT typically involved a different donor, all samples occurring after the patient received salvage FMT were excluded.

Statistical analysis for shotgun metagenomics sequencing. Microbiome sequencing data were processed and analyzed using the phyloseq package (version 1.50.0). Taxonomic assignments and abundance tables were imported into a phyloseq object, including corresponding sample metadata. α-Diversity analysis was performed using the vegan package (version 2.7.1), calculating richness and Shannon index. Principal component analysis was done with the packages prcomp (version 4.4.2) and factoextra (version 1.0.7), visualizing the variance explained by the principal components and the top contributing taxa. For the donor clusters unsupervised analysis, one sample from cluster A was removed from the visualization but included in the cluster calculation. PERMANOVA analysis was performed with 999 permutations using the 'adonis' function from the vegan package. Strain sharing between the patients and donors was calculated using StrainPhlAn4 with an in-house database for strain identification as previously published. Bray–Curtis dissimilarity was calculated between the samples and their corresponding donor samples using the 'distance' function from phyloseq. These distances were then adjusted to their corresponding baseline sample to observe the fold change over time. Linear discriminant analysis (LDA) effect size (LEfSe) was performed to identify microbial taxa that differentiate between subject groups according to their response, cohort or toxicity development using the package yingtools2 (version 0.0.1.184). We filtered taxa to be in at least 10% of the samples (prevalence cutoff of 5%). Features with LDA scores greater than 2 and $P < 0.05$ were retained. Taxonomic abundance patterns between groups were visualized via heatmaps generated by the ComplexHeatmap package (version 2.22.0). The analysis was based on differentially abundant taxa between conditions using a Wilcoxon rank-sum test.

Strain-level analysis. The strain-level analysis to assess strain engraftment was performed following the procedure previously published[23]. Phylogenetic trees were generated for each SGB with StrainPhlAn4. The thresholds on normalized phylogenetic distances to define same-strain pairs were determined for each SGB separately by comparing the distances between pairs of longitudinal samples to the pairs of unrelated samples in the corresponding phylogenetic tree, and their separation was maximized with Youden's index. Strain engraftment of an SGB was detected if the donor sample had the same strain of the SGB as the post-FMT sample.

Calculation of SGB categories. For all patients with available corresponding donor shotgun metagenomic sequencing data, SGBs in each sample were categorized as follows: 'Baseline' for the SGBs unique only to the patient at their baseline sample; 'Donor' for the SGBs present in the sample that matched unique SGBs from the respective donor sample but were not found in the baseline sample; 'Both' for unique SGBs that were found in both the baseline sample and the matching donor sample; 'New' for SGBs not present in either the 'Donor' or the 'Baseline'; and 'Lost' when SGBs that were identified at baseline were no longer present in the sample. To calculate the proportion of lost SGBs, we divided the 'Lost' SGBs by the total amount of SGBs present at baseline.

Pathway analysis from shotgun metagenomics sequencing. Shotgun metagenomic samples were also processed with the HMP Unified Metabolic Analysis Network (HUMAnN3) pipeline (version 3.8). We evaluated the stratified pathway abundances from the MetaCyc database. Pathways with zero total abundance across all samples were filtered out. Differential abundance analysis between baseline and post-FMT was performed using DESeq2 (version 1.46.0).

BiomScope pipeline

Pipeline description. Gene abundance profiling was performed using both the 10.1 million-gene integrated catalog of the human gut microbiome[59] and the 8.4 million-gene integrated reference catalog of the human oral microbiome[60]. Filtered high-quality reads were rarefied to 20 million by seqtk and then mapped with an identity threshold of 95% of each catalog using Bowtie (version 2.4.4). A gene abundance table was generated with BiomScope software[61] through a two-step procedure. First, the uniquely mapped reads (reads mapping to a single gene in the catalog) were attributed to their corresponding genes. Second, shared reads (reads that mapped with the same alignment score to multiple genes) were attributed according to the ratio of their unique mapping counts. For quantification of species, gene abundance was normalized using the fragments per kilobase of transcript per million mapped reads strategy (normalization by the gene size and the number of total mapped reads reported in frequency), and species abundance was determined from the average abundance of the first 100 core genes of each species provided in the annotation of the each million-gene catalog. Species with fewer than 10 core genes detected were counted with an abundance equal to zero. Species are reported as Metagenomic Species Pan-genomes (MSPs) that were defined and described previously[62].

Species retention. Species were first categorized for each patient according to their presence status in baseline timepoint of patient and donor, defining the following categories: both, only patient, only donor and new categories. Species never seen at any timepoint were discarded. Species were then grouped by category and filtered for at least 10 observations—for example, seen in one of the categories for at least 10 patients. The proportion of patients with the species present at a given timepoint is called the species retention. The curve displaying species retention was obtained as the median of all retention values of the different species in a specific category, with 95% confidence intervals for median. P values were calculated using the Mann–Whitney–Wilcoxon test.

High-throughput culturomics

High-throughput culturomics was done as previously performed[63]. A total of 0.3 g of stool from enrolled patients was resuspended in 1 ml of sterile 1× PBS. From this suspension, seven serial dilutions were prepared, and 50 µl of each dilution was plated onto 5% Columbia agar supplemented with sheep blood (COS; Thermo Fisher Scientific). Plates were incubated aerobically and anaerobically in an anaerobic chamber (5% H_2, 5% CO_2 and 90% N_2) at 37 °C for up to 72 hours. Anaerobic conditions were achieved using sealed Zip bags (Becton Dickinson) containing GasPak anaerobic generators (Becton Dickinson). In parallel, enrichment cultures were performed by inoculating 200 µl of stool suspension into BD BACTEC Lytic/10 Aerobic (Becton Dickinson) for aerobic conditions. For anaerobic conditions, BD BACTEC Lytic/10 Anaerobic/F (Becton Dickinson) and Yeast Casitone Fatty Acids Broth with Carbohydrates (YCFAC) were used. All broth cultures were supplemented with 5% defibrinated sheep blood and 5% filtered rumen fluid (0.22 µm). At multiple timepoints (24 hours, 3 days, 7 days, 10 days, 15 days, 21 days and 30 days), serial dilutions from enrichment broths were plated on COS agar and incubated under the same aerobic and anaerobic conditions. After incubation, isolated colonies were subcultured onto fresh COS agar and incubated at 37 °C for an additional 72 hours. Colonies were then purified and subjected to identification. Bacterial identification was performed using matrix-assisted laser desorption/ionization time-of-flight mass spectrometry (MALDI-TOF MS). For each isolate, a double spot was deposited onto a 96-spot MSP target plate, overlaid with 1 µl of a saturated α-cyano-4-hydroxycinnamic acid matrix solution (prepared in 50% acetonitrile and 2.5% trifluoroacetic acid) and allowed to dry. Spectra were acquired using a MicroFlex LT/SH mass spectrometer (Bruker) and analyzed via FlexControl version 3.4 and MALDI Biotyper Compass version 4 software. Identification was achieved by comparison to the Bruker MBT Compass BDAL reference library and an in-house spectral database. Colonies yielding identification scores higher than 1.9 were considered reliably identified at the species level. Isolates with scores lower than 1.9 were further analyzed by whole-genome sequencing for taxonomic assignment. Bacterial species detected in patient samples at baseline were compared to those identified 1 month after FMT. Due to lack of donor samples available for culturomics, we used the corresponding donor shotgun metagenomics sequencing sample. Species detected at baseline but absent at the 1-month post-FMT timepoint were classified as lost. Conversely, bacterial species present in both the donor sample and the recipient 1 month after FMT—but not detected in the patient at baseline—were defined as engrafted from the donor. Engraftment from the donor versus lost from baseline was compared using the non-parametric Mann–Whitney *U*-test using GraphPad Prism (version 10.4.2) software.

Metabolomic analysis

Fifty microliters of plasma was mixed with 500 µl of ice-cold extraction solution (methanol:water, 9:1, v/v, at −20 °C) containing isotopically labeled internal standards. The mixture was vortexed for 5 minutes at 2,500 rpm to ensure thorough homogenization and efficient extraction of endogenous metabolites. Samples were then centrifuged at 15,000*g* for 10 minutes at 4 °C. The resulting supernatants were collected and aliquoted into multiple fractions to be analyzed by different liquid chromatography coupled with mass spectrometry (LC–MS)[64]. Targeted detection of polyamines and bile acids was performed by LC–MS/MS using a 1290 Ultra-High-Performance Liquid Chromatography (UHPLC) system (Agilent Technologies) coupled to a 6470 triple quadrupole mass spectrometer (QQQ 6470) (Agilent Technologies). For polyamine quantification, 10 µl of extract was injected into a Kinetex C18 analytical column (150 mm × 2.1 mm, 2.6-µm particle size; Phenomenex), equipped with a C18 guard column (5 mm × 2.1 mm). The column was maintained at 40 °C using a Peltier oven. Chromatographic separation was achieved using a binary mobile phase consisting of (A) water with 0.1% heptafluorobutyric acid (HFBA) and (B) acetonitrile with 0.1% HFBA, both freshly prepared. The initial mobile phase composition was 95% A and 5% B, followed by a linear gradient to 30% B over 7 minutes. The column was washed with 90% B for 2.25 minutes and then re-equilibrated with 5% B for 4 minutes. The autosampler was maintained at 4 °C. Mass spectrometry parameters included gas temperature of 350 °C, gas flow rate of 12 l min^{-1} and capillary voltage of 2.5 kV. For bile acid analysis, 10 µl of sample was injected onto a Column Poroshell 120 EC-C8 1,200 bars (100 mm × 2.1 mm, 1.9-µm particle size; Agilent Technologies), protected by an XDB-C18 guard column (5 mm × 2.1 mm, 1.8 µm). The column was also maintained at 40 °C. The mobile phase consisted of (A) water with 0.2% formic acid and (B) acetonitrile:isopropanol (1:1, v/v), both freshly prepared. Initial conditions were 70% A and 30% B, followed by a shift to 38% B over 2 minutes, maintained for an additional 2 minutes. A rapid gradient from 38% to 60% B was applied over 30 seconds. The column was washed with 98% B for 2 minutes and re-equilibrated at 30% B for 1.5 minutes. Autosampler temperature was kept at 4 °C. Instrument parameters were set with gas temperature of 310 °C, gas flow rate of 9 l min^{-1} and capillary voltage of 4.5 kV. In addition, pseudo-targeted metabolomic profiling was performed using ultra-high-performance liquid chromatography coupled with high-resolution accurate mass spectrometry (UHPLC–HRAM) on a Dionex U3000 UHPLC system coupled to a Q-Exactive Orbitrap mass spectrometer (Thermo Fisher Scientific), as previously described[65,66]. All targeted treated data were merged and cleaned with a dedicated R package (@Github/Kroemerlab/GRMeta). We applied the ComBat function from the sva R package (sva version 3.52.0) to correct for inter-batch effect. Batches were divided into two groups. The batch correction model included a design matrix preserving the biological signal from key clinical covariates. Clinical features associated with samples included age, gender, body mass index (BMI), tumor type and time of first dose of ICI. ComBat was applied on $\log_{10}$-transformed AreaQCCorr values.

Statistical analysis for metabolites. Metabolite longitudinal data were analyzed using generalized additive models (GAMs) with the mgcv R package (version 1.9-3) using the 'gam' function. Each metabolite was fitted with a GAM model that included the two groups (R and NR) present in the study. Before applying any model, data were cleaned by removing individuals with only one timepoint of analysis and duplicated samples. After cleaning the dataset, this metabolite analysis comprised 100 samples from 35 patients, each having at least two timepoints sampled (from two to four). Data normalization was performed before model fitting. Metabolite intensities were transformed using square root normalization with the 'sqrt' function from R base (version 4.5). Individual GAMs were fitted for each metabolite with the following model structure:

a. Smooth terms for time with group-specific evolution over time using factor smooth interactions
b. Random effects for individual patients
c. Tweedie distribution to account for the data distribution characteristics
d. Restricted maximum likelihood (REML) estimation method

Time was modeled with penalized splines. The effective degree of freedom (edf) indicates the complexity of the time curve. In the fitted models, edf values excedeed 1, which is consistent with a nonlinear pattern. Model performance was assessed by calculating root mean squared error to evaluate model accuracy deviance explained and R^2 to assess how much the model explained the signal variance, along with residual analysis and concurvity assessment. Temporal evolution was evaluated from the fitted group-specific time smooth across the entire observation window. Reported *P* values are the significance tests for these time smooths, assessing the null hypothesis of no within-group time effect (flat curve). Temporal evolution was evaluated through model outputs and *P* value. Between-group differences

were calculated using the 'difference_smooths' function from the gratia package (version 0.10.0) to compute differences between R and NR smooth curves with 95% confidence intervals. Figures displaying temporal evolution were created using smooth estimates calculated with the 'smooth_estimates' function from the gratia package. Both trajectory and difference plots were generated using the 'ggplot' function from the ggplot2 package (version 3.5.2) and combined using the 'plot_grid' function from the cowplot package (version 1.1.3). *P* values were displayed using the 'ggsignif' function from the ggsignif package (version 0.6.4). Data manipulation was performed using the dplyr package (version 1.1.4) and tidyverse (version 2.0.0). All analyses were conducted in R (version 4.5).

Bio-Me qPCR assay

We used Precision Microbiome Profiling (PMPTM) (Bio-Me), which is a validated qPCR method for analyzing the gut microbiome composition, based on TaqMan technology on the OpenArray format (Thermo Fisher Scientific). This assay targets 108 bacterial species and subspecies (107 bacteria and one fungal species). Standard curves for the assays were created using reference materials quantified by fluorescence (Thermo Fisher Scientific, Quant-iT PicoGreen dsDNA Reagent). The reference materials were acquired from the Leibniz Institute DSMZ or the American Type Culture Collection. Standard curves for each qPCR assay were used to convert the quantification cycle (Cq) value into number of genomic copies per microliter of sample; this number was transformed into normalized absolute quantification. qPCR was performed on 220 samples in total ($n = 181$ patients and $n = 39$ donors), and only patient samples with corresponding SGB category information were included in the final analysis ($n = 104$ samples). Quantitative PCR and metagenomics relative abundance were visualized using the ComplexHeatmap package in R, and a Kendall score Kendall's τ was computed using the 'cor.test' function in the 'stat' package using pairwise complete observations. Spearman's r correlations were performed using GraphPad Prism.

Olink proteomics

Multiplex high-throughput proteomics was performed using the Immuno-Oncology Panel (Olink) and analyzed per the manufacturer's instructions. All Olink data are reported as linearized normalized protein expression (NPX), per the manufacturer's instructions. Olink data were visualized in R using the OlinkAnalyze package using 'olink_umap_plot' using manyfold approximations and projections using uniform manifold approximation and projection (UMAP) and 'olink_volcano_plot'. For volcano plots, Benjamini–Hochberg-corrected *P* values less than 0.05 were considered statistically significant.

Quantification of 16S PCR

Quantitative real-time PCR was performed to assess the relative abundance of total bacterial DNA in stool samples by targeting the V6 region of the 16S rRNA gene. The primer pair used was 891F (5′-TGGAGCATGTGGTTTAATTCGA-3′) and 1033R (5′-TGCGGGACTTA ACCCAACA-3′)[67]. For each reaction, 400 ng of extracted DNA was combined with 500 nM of each primer and 1× qPCRBIO SyGreen Blue Mix Hi-ROX (PCR Biosystems). Amplification was carried out using a real-time PCR system, and threshold cycle (Ct) values were obtained. Bacterial load was estimated by comparing sample Ct values to a standard curve generated using serial dilutions of *Escherichia coli* genomic DNA, allowing for the approximation of bacterial DNA concentration in ng μl^{-1}. Non-parametric Mann–Whitney–Wilcoxon test to compare SGB loss groups and two-way ANOVA were performed in GraphPad Prism.

Peripheral blood mononuclear cell immuno-phenotyping

Spectral flow cytometry staining and acquisition. Aliquots of cryopreserved peripheral blood mononuclear cells (PBMCs), each containing 5×10^6 cells preserved in fetal calf serum (FCS) with DMSO, were quickly thawed, gently washed and resuspended in FACS buffer consisting of 1× PBS supplemented with 5% FCS and 2 mM EDTA. To exclude non-viable cells, samples were incubated with the LIVE/DEAD Fixable Blue Dead Cell Stain Kit (Invitrogen) according to the manufacturer's protocol. Surface staining was performed using fluorochrome-conjugated antibodies sourced from BD Biosciences, R&D Systems, MBL, BioLegend, Miltenyi Biotec and Cytek (see reagent list for detailed panel composition; Supplementary Table 3). Data were acquired with a Cytek Aurora 5-laser spectral analyzer, and data analysis was performed using FlowJo version 10.8.1 software.

Manual gating and high-dimensional flow cytometry analysis. Flow cytometry analysis of PBMCs followed a sequential gating strategy that excluded debris, cell doublets and non-viable cells, ultimately selecting for viable $CD45^+$ immune cells. The resulting $CD45^+$ live-cell populations were exported as new .fcs files using FlowJo version 10.8.1, and these curated datasets served as input for UMAP and Single-cell Cytometry Annotation Network (Scyan) analyses.

Algorithms for dimensionality reduction: UMAP analysis. The UMAPs were computed and displayed using the Scanpy package[68] on alive $CD45^+$ cells.

Scyan automatic annotation. Cell type annotations were automatically performed using Scyan[69] a biology-driven model that leverages prior knowledge of cell types. This approach allowed us to identify nine main populations: basophils, natural killer cells, B cells, monocytes, dendritic cells, $CD4^+$ T cells, $CD8^+$ T cells, double-positive T cells and double-negative T cells. Subsequently, for each patient, separate .fcs files were generated for each of these nine populations. The percentages of all subpopulations were then determined through manual gating using FlowJo version 10.8.1.

Murine experiments

All animal studies were approved by the Institutional Animal Care Committee at the Centre de Recherche du Centre Hospitalier de l'Université de Montréal (CRCHUM) and carried out in compliance with Canadian Council on Animal Care guidelines (ethical protocol C22017Br). Murine experiments were conducted using 7-week-old female wild-type C57BL/6 SPF-reared mice obtained from Charles River Laboratories. Mice received 3 days of antibiotics solution containing ampicillin (1 mg ml^{-1}), streptomycin (5 mg ml^{-1}) and colistin (1 mg ml^{-1}) (Sigma-Aldrich), which was added to the sterile drinking water of mice before FMT. Three consecutive FMTs, using patient feces (ethics approval was obtained (MP-02-2022-10121/21.173, MP-02-2018-7132/17.035 and 16.161)), were performed at day −15, day −14 and day −13 (Fig. 4i). FMT was performed by thawing fecal material, and 200 µl of the suspension (100 mg ml^{-1}) was then transferred by oral gavage. An additional 100 µl was applied on the fur of each animal.

Two weeks after the first FMT, mice were implanted subcutaneously with 0.8×10^6 MCA-205 cells. When tumors reached 25–35 mm^2 in size or 35–45 mm^2 in size for anti-PD-1 monotherapy and anti-PD-1 plus anti-CTLA-4 experiments, respectively, mice were treated four times intraperitoneally every 3 days with anti-PD-1 monoclonal antibody (250 µg per mouse; Bio X Cell, clone RMP1-14) or anti-PD-1 monoclonal antibody plus anti-CTLA-4 monoclonal antibody (100 µg per mouse; Bio X Cell, clone 9D9). Additionally, the mice received a 200-µl gavage of NaCl or bacterial cocktail group starting 3 days after the tumor implantation and at each treatment. Tumor sizes were measured with manual calipers. The mice were euthanized 2 days after the last treatment. Experimental groups were compared using the Mann–Whitney–Wilcoxon test in GraphPad Prism.

Bacterial cocktail group preparation

For murine experiments, bacterial cocktails were prepared as follows. Bacterial strains used in the murine experiments were isolated

from patients at baseline enrolled in the FMT-LUMINate clinical trial and stored at −80 °C. Bacteria were cultured from frozen stocks on fastidious anaerobe agar plates (Thermo Fisher Scientific, PB0225A) for 48 hours at 37 °C under anaerobic conditions. Prior to cocktail formulation, the identity of each isolate was confirmed by MALDI-TOF MS. After identification, bacterial colonies were collected, resuspended in sterile NaCl and adjusted to an optical density of 1.0, corresponding to approximately 1×10^9 colony-forming units (CFU) per milliliter.

Cell culture, reagents and tumor cell lines

MCA-205 fibrosarcoma cells, class I MHC H-2b syngeneic cell lines for C57BL/6 mice, were used for this study and obtained from Jonathan Stagg's laboratory. The cells were cultured at 37 °C in the presence of 5% CO_2 in RPMI 1640 containing 10% FCS, 2 mM L-glutamine and 100 UI ml^{-1} penicillin–streptomycin. All reagents were purchased from Gibco-Invitrogen. Cell lines were checked for mycoplasma using PlasmoTest Mycoplasma Detection Kit (InvivoGen).

Statistical analysis

All statistical analysis and visualization were done in R or GraphPad Prism (version 10.4.2). *P* values were considered statistically significant if $P < 0.05$, and all *P* values were two-sided.

Reporting summary

Further information on research design is available in the Nature Portfolio Reporting Summary linked to this article.

Data availability

Raw FASTQ files are publicly available on the National Center for Biotechnology Information biorepository with accession number PRJNA1289847. Study-level clinical data from this study (including the protocol) will be made available upon reasonable request from a qualified medical or research professional for the specific purpose laid out in that request and may include deidentified individual participant data. A response to this data request will be made within approximately 14 days. The data for this request will be available after a data transfer agreement has been signed. Requests should be sent to the corresponding author. Patient-related data not included in the paper were generated as part of a clinical trial and are subject to patient confidentiality.

References

51. Craven, L. J. et al. Extended screening costs associated with selecting donors for fecal microbiota transplantation for treatment of metabolic syndrome-associated diseases. *Open Forum Infect. Dis.* **4**, ofx243 (2017).
52. Elkrief, A. et al. Immune-related colitis is associated with fecal microbial dysbiosis and can be mitigated by fecal microbiota transplantation. *Cancer Immunol. Res.* **12**, 308–321 (2024).
53. Eisenhauer, E. A. et al. New response evaluation criteria in solid tumours: revised RECIST guideline (version 1.1). *Eur. J. Cancer* **45**, 228–247 (2009).
54. Seymour, L. et al. iRECIST: guidelines for response criteria for use in trials testing immunotherapeutics. *Lancet Oncol.* **18**, e143–e152 (2017).
55. Freites-Martinez, A., Santana, N., Arias-Santiago, S. & Viera, A. Using the Common Terminology Criteria for Adverse Events (CTCAE - version 5.0) to evaluate the severity of adverse events of anticancer therapies. *Actas Dermosifiliogr.* **112**, 90–92 (2021).
56. Prindiville, S. A. et al. Patterns of enrollment in cancer treatment trials during the COVID-19 pandemic at National Cancer Institute-Designated Cancer Centers. *Cancer J.* **28**, 111–117 (2022).
57. Waterhouse, D. M. et al. Early impact of COVID-19 on the conduct of oncology clinical trials and long-term opportunities for transformation: findings from an American Society of Clinical Oncology Survey. *JCO Oncol. Pract.* **16**, 417–421 (2020).
58. Upadhaya, S. et al. Impact of COVID-19 on oncology clinical trials. *Nat. Rev. Drug Discov.* **19**, 376–377 (2020).
59. Plaza Onate, F. et al. Updated Metagenomic Species Pan-genomes (MSPs) of the human gastrointestinal microbiot. *Zenodo* https://zenodo.org/records/12820832 (2024).
60. Le Chatelier, E. et al. A catalog of genes and species of the human oral microbiota. *Data INRAE* https://doi.org/10.15454/WQ4UTV (2021).
61. Puller, V., Plaza Oñate, F., Prifti, E. & de Lahondès, R. Impact of simulation and reference catalogues on the evaluation of taxonomic profiling pipelines. *Microb. Genom.* **11**, 001330 (2025).
62. Plaza Oñate, F. et al. MSPminer: abundance-based reconstitution of microbial pan-genomes from shotgun metagenomic data. *Bioinformatics* **35**, 1544–1552 (2018).
63. Diop, K. et al. Coupling culturomics and metagenomics sequencing to characterize the gut microbiome of patients with cancer treated with immune checkpoint inhibitors. *Gut Pathog.* **17**, 21 (2025).
64. Grajeda-Iglesias, C. et al. Oral administration of *Akkermansia muciniphila* elevates systemic antiaging and anticancer metabolites. *Aging (Albany NY)* **13**, 6375–6405 (2021).
65. Durand, S. et al. The intracellular metabolome of starving cells. *Methods Cell Biol.* **164**, 137–156 (2021).
66. Abdellatif, M. et al. Nicotinamide for the treatment of heart failure with preserved ejection fraction. *Sci. Transl. Med.* **13**,eabd7064 (2021).
67. Anhê, F. F. et al. Treatment with camu camu (*Myrciaria dubia*) prevents obesity by altering the gut microbiota and increasing energy expenditure in diet-induced obese mice. *Gut* **68**, 453–464 (2019).
68. Wolf, F. A., Angerer, P. & Theis, F. J. SCANPY: large-scale single-cell gene expression data analysis. *Genome Biol.* **19**, 15 (2018).
69. Blampey, Q. et al. A biology-driven deep generative model for cell-type annotation in cytometry. *Brief. Bioinform.* **24**,bbad260 (2023).

Acknowledgements

The authors thank the patients, their families and their caregivers. This study was funded by the Canadian Cancer Society Impact Grant. The study was also partially funded by the Weston Family Foundation (Weston Family Foundation Proof-of-Concept Grant). We thank the Unité d'Innovations Thérapeutiques at the CRCHUM. We thank the staff at the CRCHUM animal facility and the immunomonitoring facility. We thank the staff at Génome Québec. A.E. was supported by the Seerave Foundation, the Fonds de recherche Québec–Santé (FRQS) Clinician Scientist Award, the Canadian Cancer Society, the Cancer Research Society Next Generation of Scientists and the Society of Immunotherapy of Cancer–Melanoma Research Alliance Women in Melanoma Award. For the present work, A.E. was also partially supported by the Guy Lafleur Foundation, the Institut de Cancer de Montréal and the ASCO Conquer Cancer Foundation Young Investigator Award. B.R. is supported by the Seerave Foundation, the Canadian Cancer Society and the FRQS Clinician Scientist Award. S.M.V. received salary support from the Ontario Institute of Cancer Research and the London Health Sciences Foundation Helen and Andy Spriet funds. M.S. received grant support for this work from the St. Joseph's Health Care Foundation. L.D. is supported by the 2025 AACR Career Development Award in Lung Cancer Research and by the Association Robert Debré pour la Recherche Médicale. L.Z. is funded by the European Research Council (ERC) under grant agreement no. 101052444. L.Z. and L.D. are supported by the Seerave Foundation, the European Union's Horizon Europe research and innovation program under grant agreement no. 101095604 (project acronym: PREVALUNG-EU, project title: Personalized lung cancer risk assessment leading to stratified interception), the European

Union's Horizon 2020 research and innovation program under grant agreement no. 825410 (ONCOBIOME project), the European Union's Horizon 2020 research and innovation program under grant agreement no. 964590 (project acronym: IHMCSA, project title: International Human Microbiome Coordination and Support Action. ANR Ileobiome - 19-CE15-0029-01, ANR RHU5 'ANR-21-5 RHUS-0017' IMMUNOLIFE, MAdCAM INCA_16698 and Ligue contre le cancer). L.D. was also funded by the SIGN'IT ARC Foundation (MICROBIONT-PREDICT (2021)). G.K. is supported by the Ligue contre le Cancer (équipes labellisées); Agence Nationale de la Recherche (ANR) under the France 2030 program (reference no. 21-ESRE-0028, ESR/Equipex+ Onco-Pheno-Screen; program RHU ANR-21-RHUS-0017 IMMUNOLIFE and ANR-23-RHUS-0010 LUCA-pi; ANR-22-CE14-0066 VIVORUSH, ANR-23-CE44-0030 COPPERMAC, ANR-23-R4HC-0006 Ener-LIGHT), an ERC Advanced Investigator Award (ERC-2021-ADG, grant no. 101052444; project acronym: ICD-Cancer); the Hevolution Network on Senescence in Aging (reference HF-E Einstein Network); European Union Horizon 2020 research and innovation programs Oncobiome (grant agreement no. 825410) and Prevalung (grant agreement no. 101095604), Institut National du Cancer (INCa), Institut Universitaire de France; PAIR-Obésité INCa_18713, Seerave Foundation, SIRIC Cancer Research and Personalized Medicine (CARPEM, SIRIC CARPEM INCa-DGOS-Inserm-ITMO Cancer_18006 supported by Institut National du Cancer, Ministère des Solidarités et de la Santé and INSERM). This study (Immuno-Onco) contributes to the IdEx Université de Paris Cité ANR-18-IDEX-0001.

Author contributions

Conceptualization: A.E., B.R. and S.M.V. Methodology: all authors. Investigation: all authors. Formal analysis: S.D., S.H., M.M., M.F., A.D., I.B., D.S., D.R., M.G., G.P., M.P., A.F., V.H., R.L. and V.P. Data curation: A.D., I.B., W.B., N.B., M.T., S.O., K.B., B.S., J.R., J.L., D.B., N.M., D.K.P., N.R., S.N., F.P. and F.A. Resources: all authors. Writing—original draft: A.E., B.R. and S.D. Writing—review and editing: all authors. Visualization: all authors. Supervision: A.E. and B.R. Project administration: A.E., B.R. and S.M.V. Funding acquisition: A.E., B.R. and S.M.V.

Competing interests

A.D. received research funding from AstraZeneca, Exelixis, Regeneron and Fondation Saputo; advisory board and consulting fees from Boehringer Ingelheim, EMD Serono, Merck and Johnson & Johnson/Janssen; and speaker honoraria from Boehringer Ingelheim and AstraZeneca. A.E. declares grant support from Kanvas Biosciences, GMT Science, AstraZeneca, Merck and Bristol Myers Squibb. A.E. declares honoraria from AstraZeneca, Merck, Bristol Myers Squibb and EMD Soreno. A.E. declares consulting fees from EverImmune, NECBio and Sanofi-Pasteur. A.E. is inventor on patent 4872-8531-1934.1 regarding the microbiome and immunotherapy response. B.R. declares research funding from Davolterra and Kanvas Biosciences and consulting fees from Merck, AstraZeneca, EverImmune and Bristol Myers Squibb. B.R. is also a co-founder of Curebiota. S.M.V. reports a grant from Microviable Therapeutics outside the submitted work as well as consulting fees from Kanvas Biosciences and FedBio. S.M.V. is a co-founder of LND Therapeutics, Inc., which holds the rights to LND101. S.M.V. reports US Patent Application No. 63/913,940 related to FMT donor screening. M.S. is a co-founder of LND Therapeutics, Inc., which holds the rights to LND101. M.S. reports US Patent Application No. 63/913,940 related to FMT donor screening. S.P. is a co-founder of LND Therapeutics, Inc., which holds the rights to LND101. G.K. has been holding research contracts with Daiichi-Sankyo, Eleor, Kaleido, Lytix Pharma, PharmaMar, Osasuna Therapeutics, Samsara Therapeutics, Sanofi, Sutro, Tollys and Vascage. G.K. is on the Board of Directors of Bristol Myers Squibb Foundation France. G.K. is a scientific co-founder of EverImmune, Osasuna Therapeutics, Samsara Therapeutics and Therafast Bio. G.K. is on the scientific advisory boards of Hevolution, Institut Servier and Rejuveron Life Sciences/Centenara Labs AG. G.K. is the inventor of patents covering therapeutic targeting of aging, cancer, cystic fibrosis and metabolic disorders. Among these patents, one, 'Methods for weight reduction' (US11905330B1), is relevant to this study. A close family member of G.K. was an employee of Sanofi and now consults for Boehringer Ingelheim. J.R. reports participating in advisory boards for Merck, AstraZeneca, Lilly and Novartis. S.O. reports honoraria/consulting fees from AstraZeneca, Amgen, Bristol Myers Squibb, Boehringer Ingelheim, Janssen, Merck, Pfizer and Roche. The other authors declare no competing interests.

Additional information

Extended data is available for this paper at https://doi.org/10.1038/s41591-025-04186-5.

Supplementary information The online version contains supplementary material available at https://doi.org/10.1038/s41591-025-04186-5.

Correspondence and requests for materials should be addressed to Arielle Elkrief.

Peer review information *Nature Medicine* thanks Diwakar Davar, Jun Zhang and the other, anonymous, reviewer(s) for their contribution to the peer review of this work. Primary Handling Editor: Saheli Sadanand, in collaboration with the *Nature Medicine* team.

https://doi.org/10.1038/s41591-025-04186-5

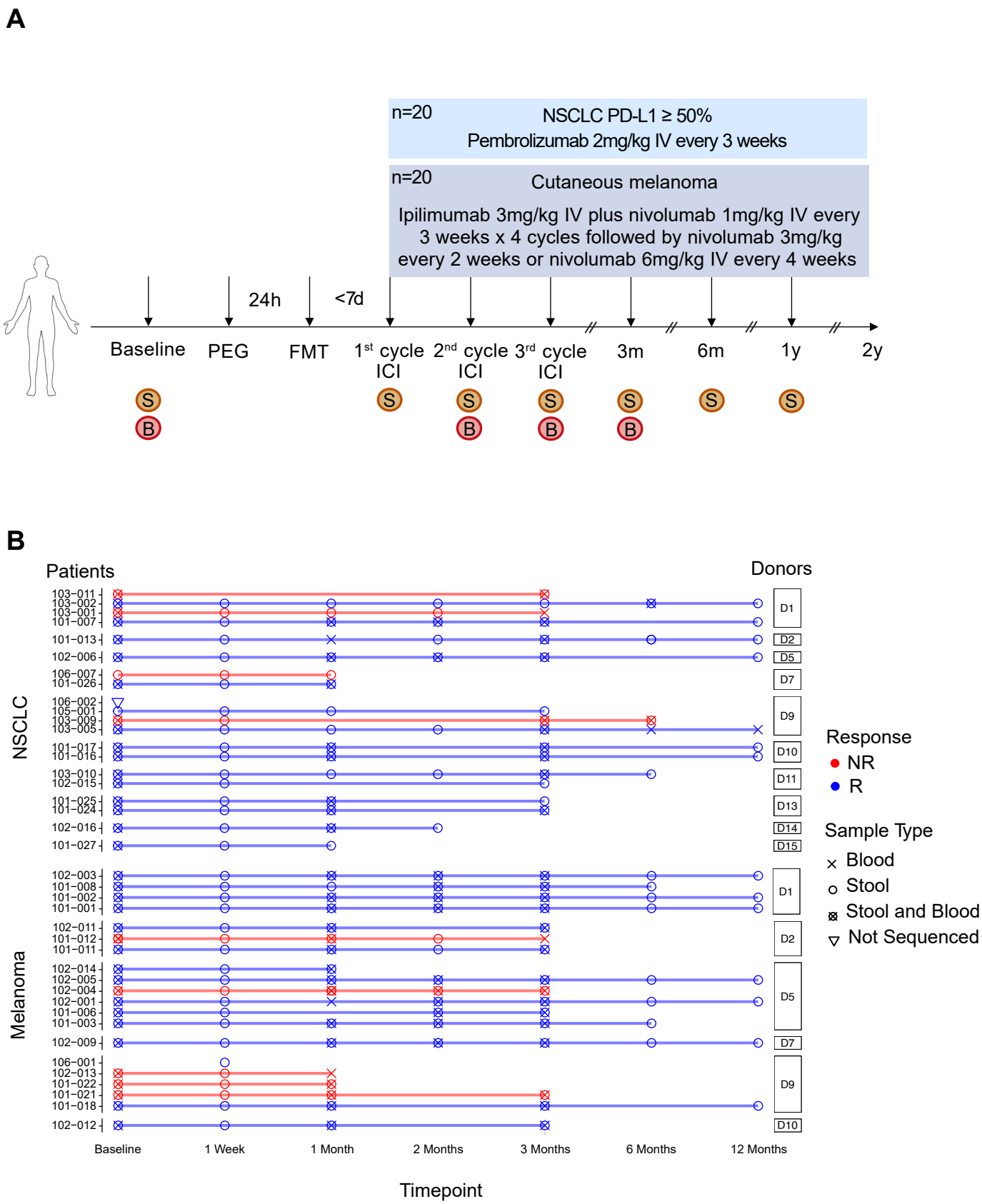

Extended Data Fig. 1 | Trial Design. A. Trial design **B.** Sample manifest and corresponding donor. S; stool sample. B; blood sample. R; responder. NR; non-responder. PEG; polyethylene glycol bowel preparation. ICI; immune checkpoint inhibitors.

https://doi.org/10.1038/s41591-025-04186-5

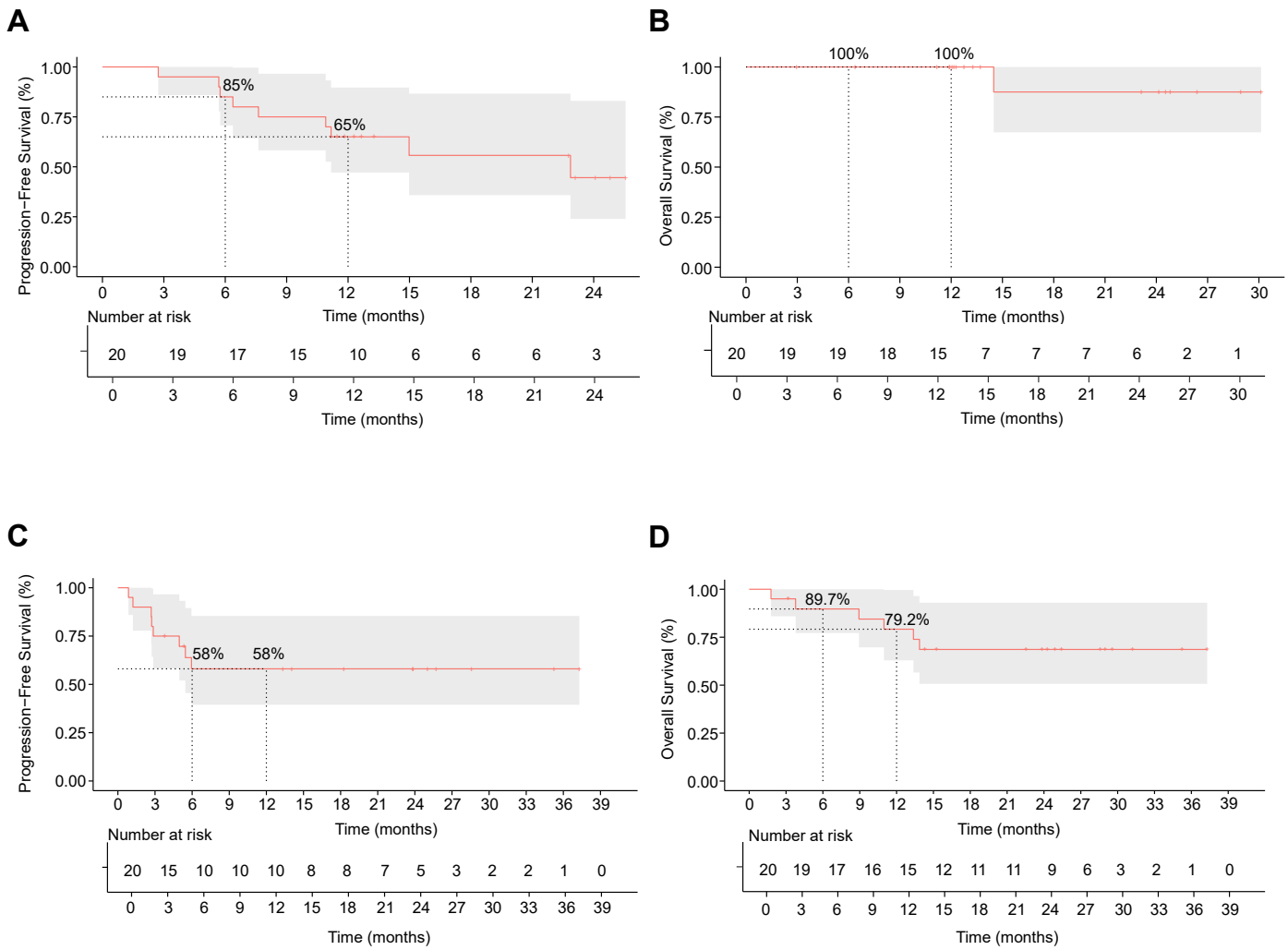

Extended Data Fig. 2 | Progression-free and overall survival. Kaplan-Meier estimates for patients in the NSCLC cohort for **A.** Progression-free survival and **B.** Overall survival. Kaplan-Meier estimates for patients in the melanoma cohort for **C.** Progression-free survival and **D.** Overall survival.

https://doi.org/10.1038/s41591-025-04186-5

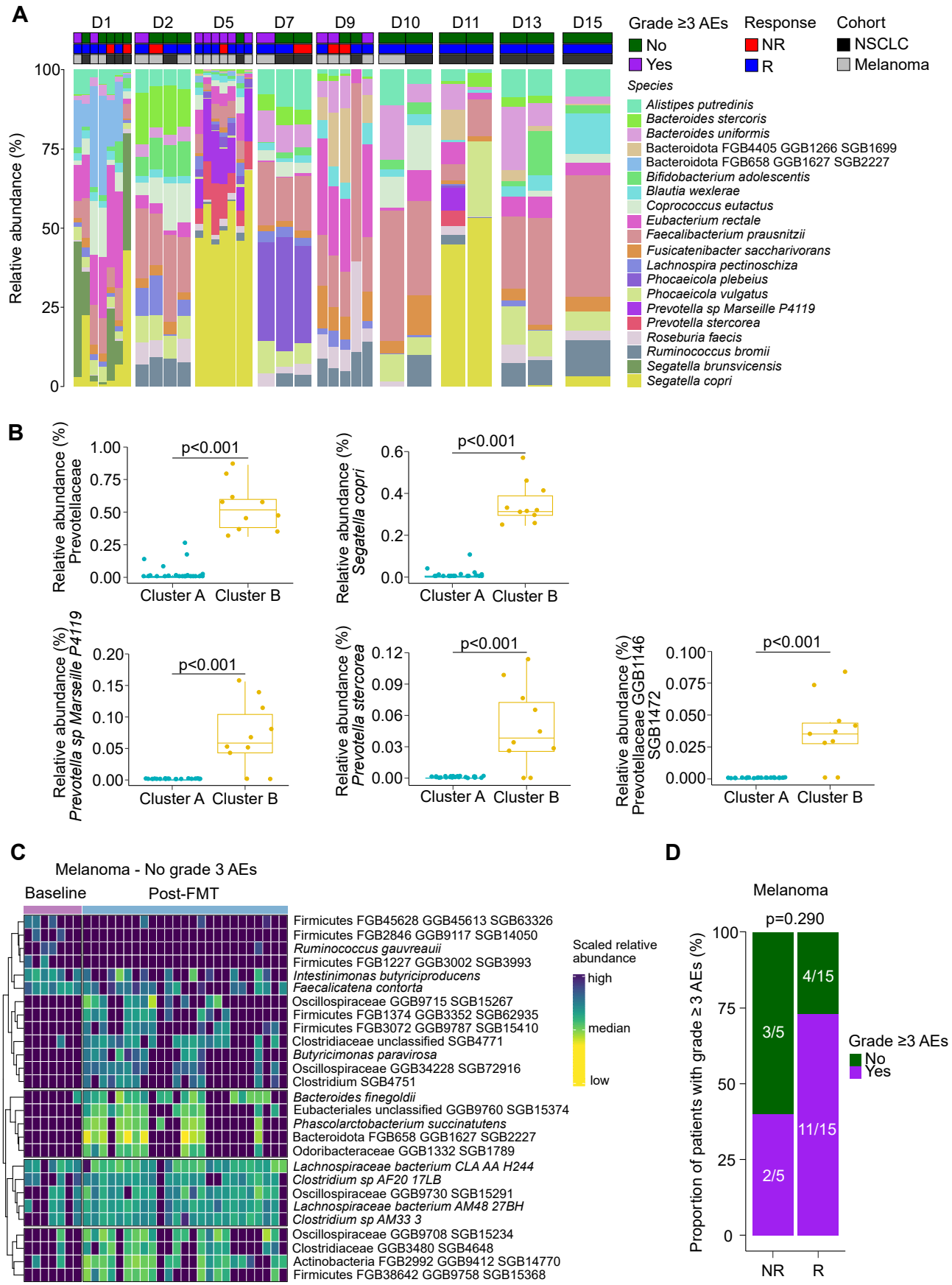

Extended Data Fig. 3 | See next page for caption.

https://doi.org/10.1038/s41591-025-04186-5

Extended Data Fig. 3 | Donor metagenomic profiling and association with immune-related adverse events. A. Relative abundance of donor samples using metagenomic sequencing; represented by a stacked-barplot of the proportionally distributed top 20 relative abundant species shown. **B**. Relative abundance of *Prevotella spp* according to donor cluster. (n = 23 in Cluster A and 10 in Cluster B), p-value computed by Wilcoxon test (two-sided). (Exact p value for each graph is as follows: *Prevotellaceae* $p = 4.9e^{-06}$, *Segatella copri* $p = 2.5e^{-06}$, *Prevotella stercorea* $p = 1.9e^{-06}$, *Prevotella sp Marseille P4119* $p = 1.9e^{-06}$, *Prevotellaceae GGB1146 SGB1472* $p = 1.9e^{-06}$) **C**. Heatmap representation comparing patients without grade ≥ 3 AEs at baseline vs post-FMT (n = 32 samples from n = 7 patients). Bacteria with a $p < 0.05$ according to Wilcoxon test between timepoints shown in the heatmaps. **D**. Proportion of patients with grade ≥ 3 AEs in the melanoma cohort according to response status. Group differences were assessed using Fisher Test (two-sided). For box plots (**B**), the center line represents the median, box bounds represent the interquartile range (IQR), whiskers extend to 1.5 x IQR, and each dot represents an individual patient sample. NR; non-responder. R; responder.

https://doi.org/10.1038/s41591-025-04186-5

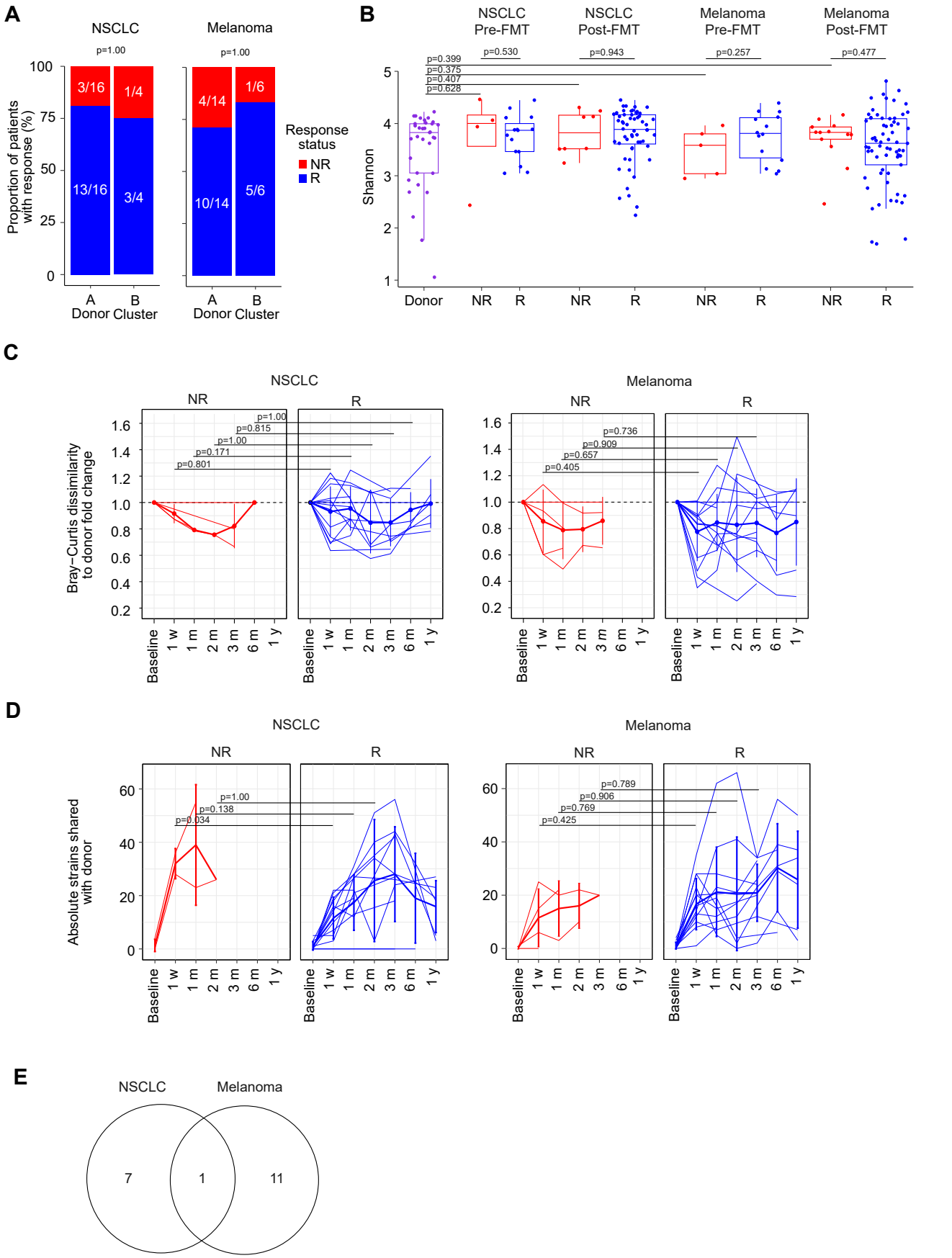

Extended Data Fig. 4 | See next page for caption.

https://doi.org/10.1038/s41591-025-04186-5

Extended Data Fig. 4 | Species and strain-level dynamics and association with response. A. Response status according to donor cluster for NSCLC and melanoma. Group differences were assessed using Fisher test (two-sided). **B**. Alpha diversity measured by the Shannon index comparing donors, responders, and non-responders at baseline versus post-FMT (n = 180 samples from n = 39 patients and 9 donors). **C**. Bray-Curtis dissimilarity to donor fold change over time (n = 182 samples from n = 37 patients) and **D**. absolute strains shared with the donor for NSCLC and melanoma cohorts in non-responders vs. responders (n = 156 samples from n = 34 patients), data are presented as mean values ± SD, for strain-sharing analysis only samples which successfully processed through the StrainPhlAn4 pipeline. **E**. Visualisation of overlap between enriched species in responders post-FMT from LEfSe analysis. For box plots (**B**), the center line represents the median, box bounds represent the interquartile range (IQR), whiskers extend to 1.5 x IQR, and each dot represents an individual patient sample. R; responder. NR; non-responder. P-values for panels **B**–**D** are pair-wise comparison using Wilcoxon test (two-sided).

https://doi.org/10.1038/s41591-025-04186-5

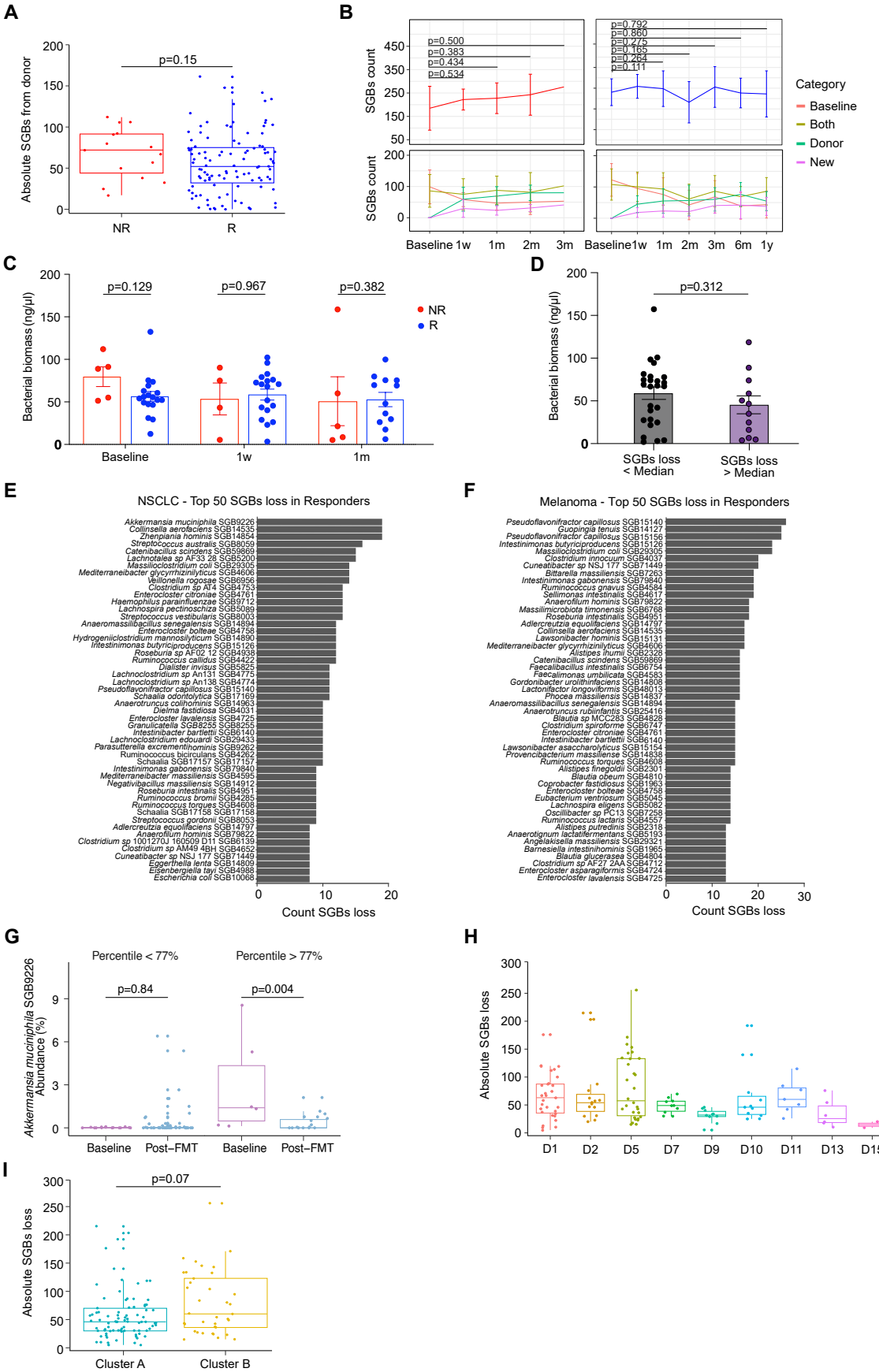

Extended Data Fig. 5 | See next page for caption.

https://doi.org/10.1038/s41591-025-04186-5

Extended Data Fig. 5 | Association between alpha diversity, strain engraftment, and Bray-Curtis dissimilarity with clinical outcome. A. Absolute SGBs engrafted from the donor in non-responders compared to responders using shotgun metagenomic sequencing (n = 122 samples from n = 32 patients), p-value computed by Wilcoxon test (two-sided). **B**. Absolute SGBs count over time in responders compared to non-responders; top plot represents in the sum of all the SGB categories, data are presented as mean values ± SD, **C**. Bacterial biomass using qPCR analysis of the 16 s rRNA gene according to response and timepoint (n = 70 samples from n = 24 patients), p-value calculated by Non-parametric Mann–Whitney U test (two-sided), data are presented as mean values ± SEM and **D**. according to SGBs loss from baseline category obtained using the median value from the metagenomics analysis (n = 38 samples from n = 22 patients), p-value calculated by Non-parametric Mann–Whitney U test (two-sided), data are presented as mean values ± SEM. Top 50 lost SGBs post-FMT in responders for **E**. NSCLC (n = 62 samples from n = 13 patients) and **F**. melanoma (n = 71 samples from n = 13 patients). **G**. Relative abundance of *Akkermansia muciniphila* across relative abundance >77th percentile vs. <77th percentile pre vs. post-FMT in responders. Absolute lost SGBs in patients post-FMT according to **H**. donor and **I**. donor cluster. For box plots (**A**, **G**–**I**), the center line represents the median, box bounds represent the interquartile range (IQR), whiskers extend to 1.5 x IQR, and each dot represents an individual patient sample.

https://doi.org/10.1038/s41591-025-04186-5

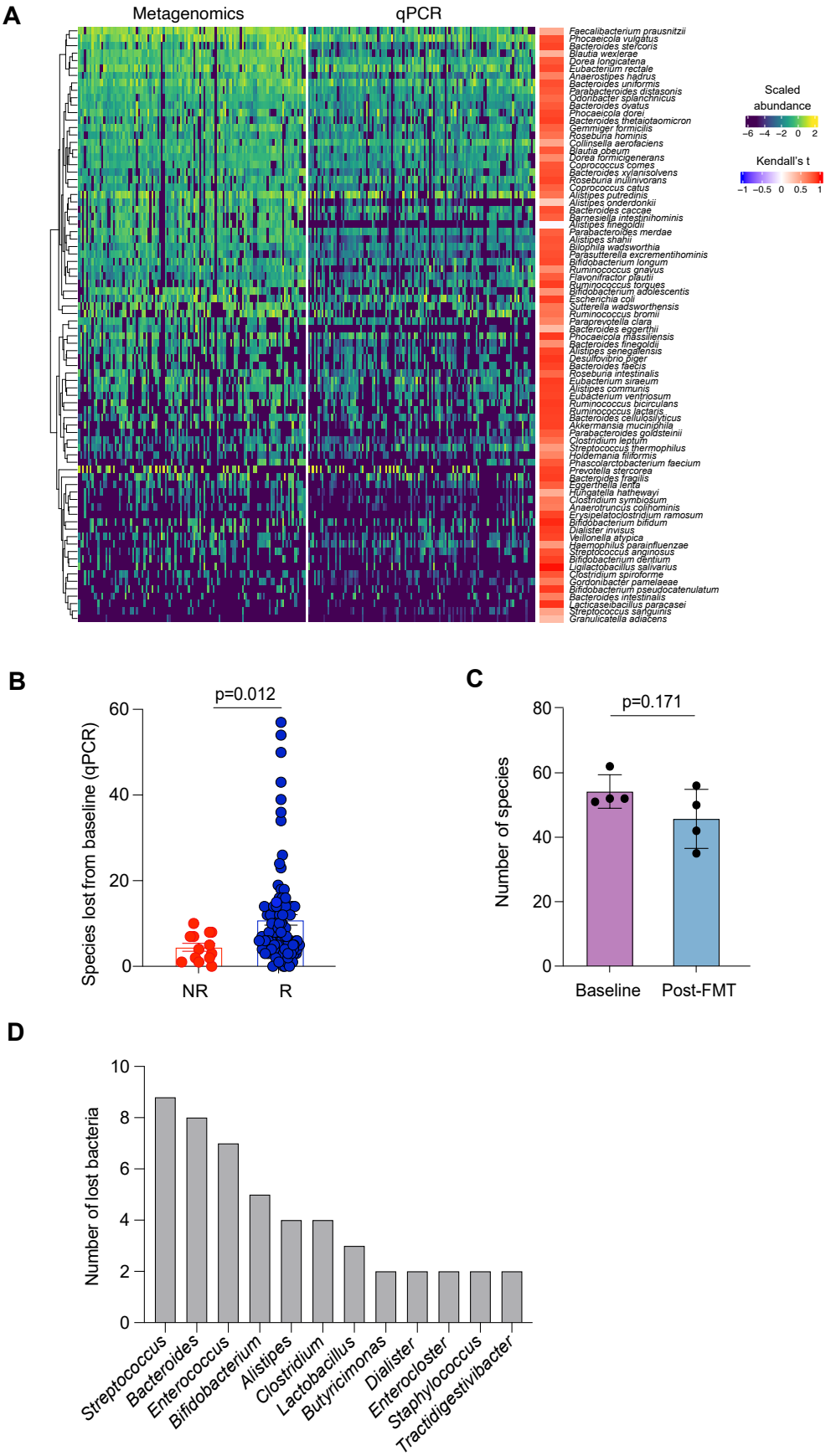

Extended Data Fig. 6 | See next page for caption.

https://doi.org/10.1038/s41591-025-04186-5

Extended Data Fig. 6 | SGBs loss as measured by qPCR and cultutomics. **A**. Heatmap representation of metagenomics and qPCR with Kendall score (n = 118 samples from n = 31 patients). **B**. Species lost post-FMT as determined by qPCR between non-responders and responders (n = 91 R and n = 13 NR for n = 28 patients), p-value calculated by Non-parametric Mann–Whitney U test (two-sided), data are presented as mean values ± SEM. **C**. Culturomics analysis of the number of species isolated from n = 4 patients at baseline (n = 4 samples) compared to post-FMT (n = 4 samples) p-value calculated by Non-parametric Mann–Whitney U test (two-sided), data are presented as mean values ± SEM. **D**. culturomics analysis of the number of bacteria initially present in the patient's baseline sample and no longer detected in the post-FMT sample, p-value calculated by Non-parametric Mann–Whitney U test (two-tailed).

https://doi.org/10.1038/s41591-025-04186-5

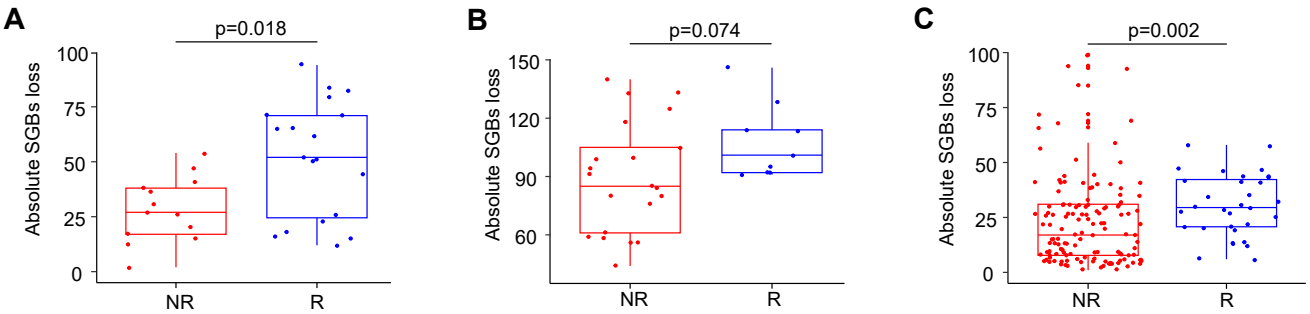

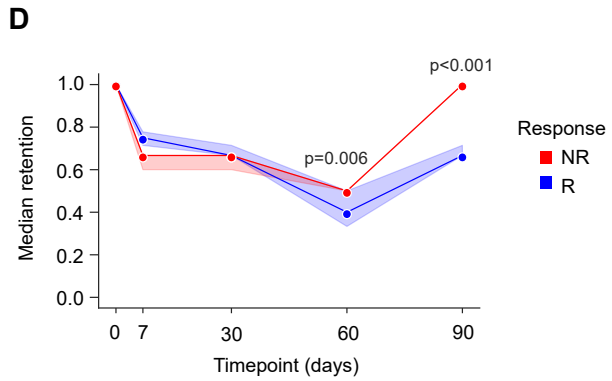

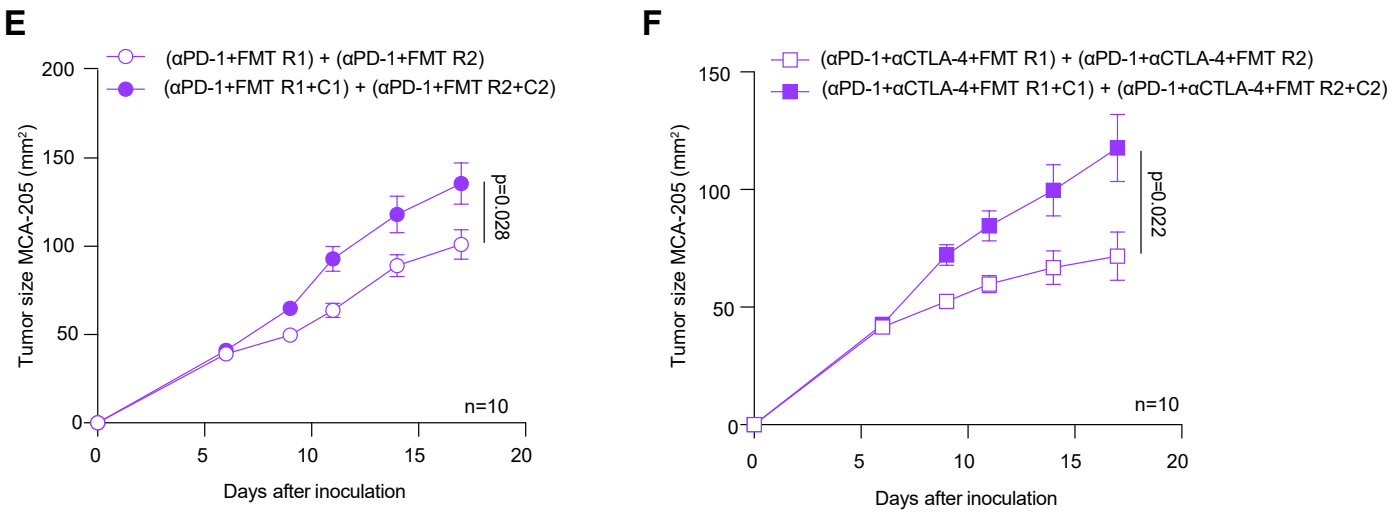

Extended Data Fig. 7 | Bacterial loss accross independent datasets and in vivo proof-of-concept. Metagenomics analysis using the MetaPhlAn4 pipeline of absolute lost SGBs in non-responders compared to responders in **A**. MIMIC (n = 32 samples from n = 12 patients), **B**. Baruch et al., (n = 30 samples from n = 10 patients) **C**. Davar et al. (n = 168 samples from n = 15 patients), p-values for panel A-C computed by Wilcoxon test (two-sided). **D**. Metagenomics analysis using the BiomScope pipeline, for each patient, species were categorized according to their presence status in the patient at baseline and their donor: "only patient" category is shown, which represent the species present in patient at baseline and not in the donor. For each species, the retention was estimated as the proportion of patients where the species is still present at the considered timepoint. Retention across species is shown over time. Pooled data from MIMIC, FMT-LUMINate, Baruch et al., and Davar et al., 95% confidence intervals for median shown; p-values were calculated using Mann-Whitney-Wilcoxon test (two-sided), data from n = 250 samples from n = 64 patients. **E**, **F**. Tumor kinetics for n = 10 mice per group, results from three independent experiments, p-value calculated by Non-parametric Mann–Whitney Wilcoxon test (two-tailed), data are presented as mean values ± SEM. For box plots (**A**–**C**), the center line represents the median, box bounds represent the interquartile range (IQR), whiskers extend to 1.5 x IQR, and each dot represents an individual patient sample. R; responder. NR; non-responder. C; cocktail.

https://doi.org/10.1038/s41591-025-04186-5

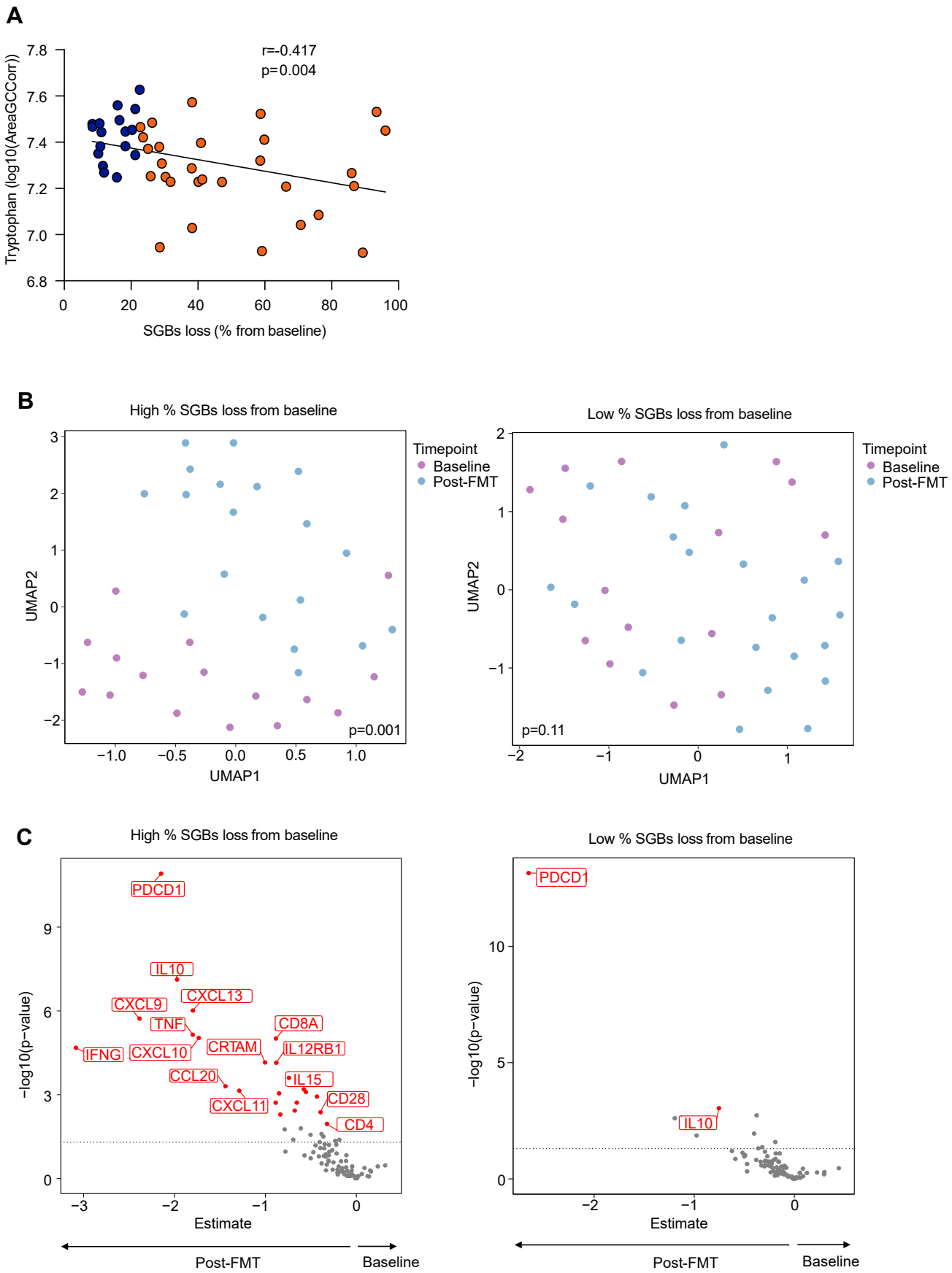

Extended Data Fig. 8 | See next page for caption.

https://doi.org/10.1038/s41591-025-04186-5

Extended Data Fig. 8 | SGBs loss modulates tryptophan levels and the plasma cytokine profile. A. Tryptophan metabolite according to SGBs loss calculated from the patient's baseline (n = 46 samples from n = 23 patients), p-value calculated by Spearman r correlation (two-sided) **B.** Olink proteomics assay UMAP representation in patients with high percentage of bacterial loss according to baseline, defined by the median, compared to low percentage of bacterial loss according to baseline, p-value calculated by one-way ANOVA (two-sided) **C.** Volcano plot of significantly enriched proteins post-FMT compared to baseline (n = 35 samples from n = 15 patients for patients with high loss and n = 37 samples from n = 16 patients for patients with low loss), p-value calculated by Welch 2-sample t-test (two-sided), corrected for multiple testing by the Benjamini-Hochberg method.

https://doi.org/10.1038/s41591-025-04186-5

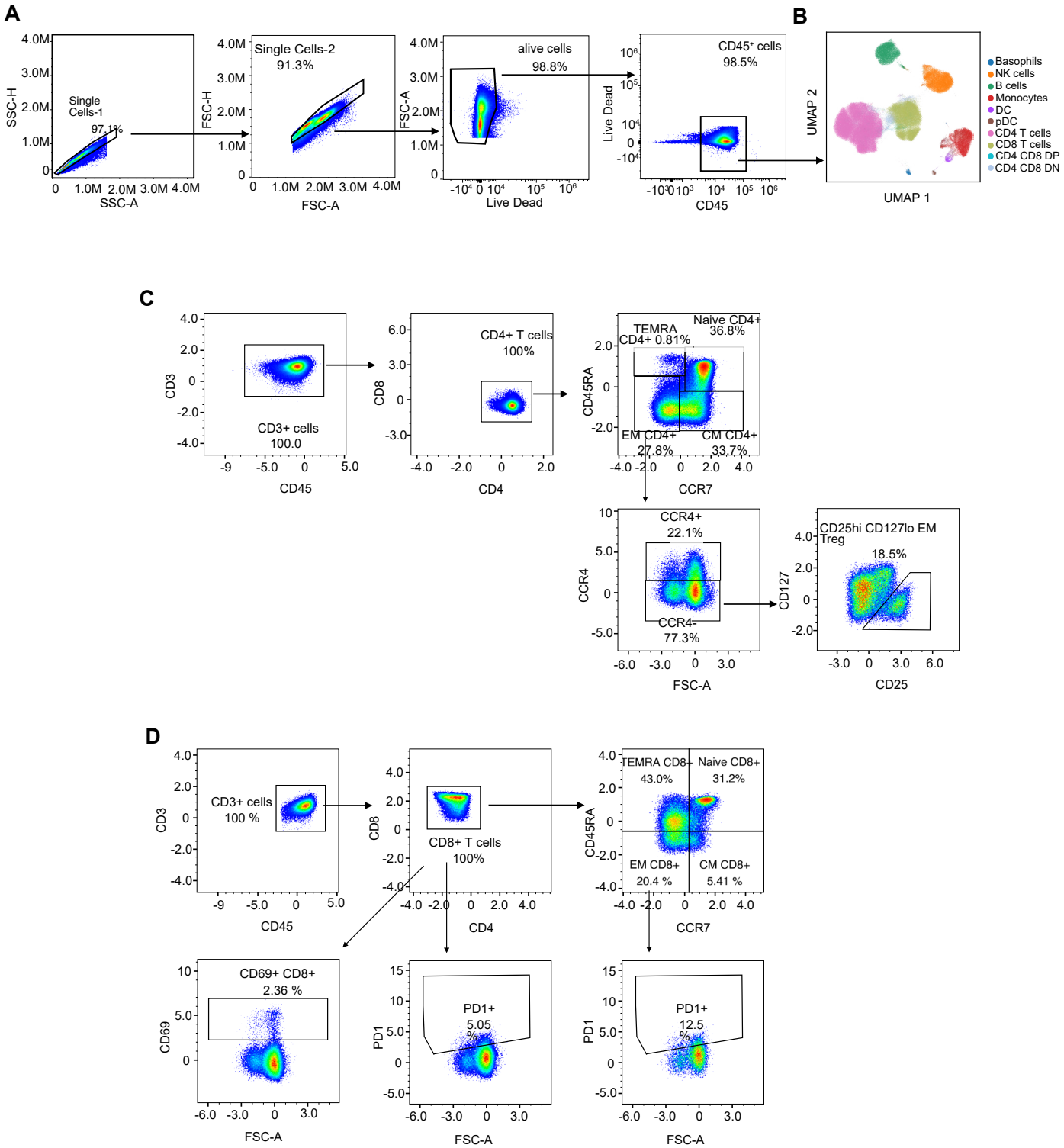

Extended Data Fig. 9 | Gating for flow cytometry on patient PBMCs. **A**. Detailed gating for CD45$^+$ cells, **B**. Non-linear dimension reduction on cell populations across all patients was applied and displayed through UMAP using automatic annotation with Scyan Python module, based-on expression matrix of characteristic markers for main populations. **C**. Detailed gating for CD4$^+$ T cell and **D**. detailed gating for CD8$^+$ T cells.

https://doi.org/10.1038/s41591-025-04186-5

Extended Data Table 1 | Safety of FMT in combination with ICI[a]

Non-Small Cell Lung Cancer Cohort (n=20)					
FMT attributable adverse events[b]					
Adverse event	**Any grade**	**Grade 1**	**Grade 2**	**Grade 3**	**Grade 4**
	5 (25.0%)	**5 (25.0%)**	**0 (0.0%)**	**0 (0.0%)**	**0 (0.0%)**
Changes in stool appearance	2 (10.0%)	2 (10.0%)	0 (0.0%)	0 (0.0%)	0 (0.0%)
Diarrhea	2 (10.0%)	2 (10.0%)	0 (0.0%)	0 (0.0%)	0 (0.0%)
FMT plus ICI attributable adverse events					
Adverse event	**Any grade**	**Grade 1**	**Grade 2**	**Grade 3**	**Grade 4**
	17 (85.0%)	**15 (75.0%)**	**8 (40.0%)**	**0 (0.0%)**	**0 (0.0%)**
Fatigue	6 (30.0%)	5 (25.0%)	1 (5.0%)	0 (0.0%)	0 (0.0%)
Rash maculo-papular	5 (25.0%)	5 (25.0%)	0 (0.0%)	0 (0.0%)	0 (0.0%)
Diarrhea	4 (20.0%)	4 (20.0%)	0 (0.0%)	0 (0.0%)	0 (0.0%)
Pruritus	4 (20.0%)	4 (20.0%)	0 (0.0%)	0 (0.0%)	0 (0.0%)
Changes in stool appearance	2 (10.0%)	2 (10.0%)	0 (0.0%)	0 (0.0%)	0 (0.0%)
Nausea	2 (10.0%)	2 (10.0%)	0 (0.0%)	0 (0.0%)	0 (0.0%)
Alanine aminotransferase increased	1 (5.0%)	0 (0.0%)	1 (5.0%)	0 (0.0%)	0 (0.0%)
Arthritis	1 (5.0%)	0 (0.0%)	1 (5.0%)	0 (0.0%)	0 (0.0%)
Bullous dermatitis	1 (5.0%)	0 (0.0%)	1 (5.0%)	0 (0.0%)	0 (0.0%)
Dyspnea	1 (5.0%)	0 (0.0%)	1 (5.0%)	0 (0.0%)	0 (0.0%)
Edema limbs	1 (5.0%)	0 (0.0%)	1 (5.0%)	0 (0.0%)	0 (0.0%)
Esophageal pain	1 (5.0%)	1 (5.0%)	0 (0.0%)	0 (0.0%)	0 (0.0%)
Hypothyroidism	1 (5.0%)	0 (0.0%)	1 (5.0%)	0 (0.0%)	0 (0.0%)
Pain	1 (5.0%)	0 (0.0%)	1 (5.0%)	0 (0.0%)	0 (0.0%)
Pancreatitis[c]	1 (5.0%)	0 (0.0%)	1 (5.0%)	0 (0.0%)	0 (0.0%)
Pneumonia	1 (5.0%)	0 (0.0%)	1 (5.0%)	0 (0.0%)	0 (0.0%)
Pneumonitis	1 (5.0%)	0 (0.0%)	1 (5.0%)	0 (0.0%)	0 (0.0%)
Cutaneous melanoma (n=20)					
FMT attributable adverse events[d]					
Adverse event	**Any grade**	**Grade 1**	**Grade 2**	**Grade 3**	**Grade 4**
	7 (35.0%)	**7 (35.0%)**	**0 (0.0%)**	**0 (0.0%)**	**0 (0.0%)**
Diarrhea	4 (20.0%)	4 (20.0%)	0 (0.0%)	0 (0.0%)	0 (0.0%)
Bloating	2 (10.0%)	2 (10.0%)	0 (0.0%)	0 (0.0%)	0 (0.0%)
Nausea	2 (10.0%)	2 (10.0%)	0 (0.0%)	0 (0.0%)	0 (0.0%)
FMT plus ICI attributable adverse events					
Adverse event	**Any grade**	**Grade 1**	**Grade 2**	**Grade 3**	**Grade 4**
	19 (95.0%)	**17 (85.0%)**	**10 (50.0%)**	**12 (60.0%)**	**1 (5.0%)**
Diarrhea	11 (55.0%)	5 (25.0%)	3 (15.0%)	3 (15.0%)	0 (0.0%)
Fatigue	8 (40.0%)	8 (40.0%)	0 (0.0%)	0 (0.0%)	0 (0.0%)
Nausea	5 (25.0%)	4 (20.0%)	1 (5.0%)	0 (0.0%)	0 (0.0%)
Rash maculo-papular	5 (25.0%)	2 (10.0%)	3 (15.0%)	0 (0.0%)	0 (0.0%)
Anorexia	4 (20.0%)	4 (20.0%)	0 (0.0%)	0 (0.0%)	0 (0.0%)
Pruritus	4 (20.0%)	4 (20.0%)	0 (0.0%)	0 (0.0%)	0 (0.0%)
Alanine aminotransferase increased	3 (15.0%)	0 (0.0%)	0 (0.0%)	3 (15.0%)	0 (0.0%)
Aspartate aminotransferase increased	3 (15.0%)	0 (0.0%)	2 (10.0%)	1 (5.0%)	0 (0.0%)
Chills	3 (15.0%)	3 (15.0%)	0 (0.0%)	0 (0.0%)	0 (0.0%)
Myocarditis	3 (15.0%)	0 (0.0%)	0 (0.0%)	2 (10.0%)	1 (5.0%)
Vomiting	3 (15.0%)	2 (10.0%)	1 (5.0%)	0 (0.0%)	0 (0.0%)
Bloating	2 (10.0%)	2 (10.0%)	0 (0.0%)	0 (0.0%)	0 (0.0%)
Colitis	2 (10.0%)	0 (0.0%)	1 (5.0%)	1 (5.0%)	0 (0.0%)
Dry mouth	2 (10.0%)	2 (10.0%)	0 (0.0%)	0 (0.0%)	0 (0.0%)
Dry skin	2 (10.0%)	1 (5.0%)	1 (5.0%)	0 (0.0%)	0 (0.0%)
Fever	2 (10.0%)	1 (5.0%)	0 (0.0%)	1 (5.0%)	0 (0.0%)
Generalized muscle weakness	2 (10.0%)	1 (5.0%)	1 (5.0%)	0 (0.0%)	0 (0.0%)
GGT increased	2 (10.0%)	1 (5.0%)	0 (0.0%)	1 (5.0%)	0 (0.0%)
Headache	2 (10.0%)	2 (10.0%)	0 (0.0%)	0 (0.0%)	0 (0.0%)
Mucositis oral	2 (10.0%)	1 (5.0%)	1 (5.0%)	0 (0.0%)	0 (0.0%)
Pneumonitis	2 (10.0%)	0 (0.0%)	1 (5.0%)	1 (5.0%)	0 (0.0%)
Weight loss	2 (10.0%)	1 (5.0%)	1 (5.0%)	0 (0.0%)	0 (0.0%)
Alkaline phosphatase increased	1 (5.0%)	0 (0.0%)	1 (5.0%)	0 (0.0%)	0 (0.0%)
Autoimmune hepatitis	1 (5.0%)	0 (0.0%)	1 (5.0%)	0 (0.0%)	0 (0.0%)
Back pain	1 (5.0%)	1 (5.0%)	0 (0.0%)	0 (0.0%)	0 (0.0%)
Dizziness	1 (5.0%)	0 (0.0%)	1 (5.0%)	0 (0.0%)	0 (0.0%)
Gastritis	1 (5.0%)	0 (0.0%)	1 (5.0%)	0 (0.0%)	0 (0.0%)
Hepatitis	1 (5.0%)	0 (0.0%)	0 (0.0%)	1 (5.0%)	0 (0.0%)
Hyperthyroidism	1 (5.0%)	1 (5.0%)	0 (0.0%)	0 (0.0%)	0 (0.0%)
Lymph node pain	1 (5.0%)	0 (0.0%)	1 (5.0%)	0 (0.0%)	0 (0.0%)
Skin hypopigmentation	1 (5.0%)	0 (0.0%)	1 (5.0%)	0 (0.0%)	0 (0.0%)
Thyroiditis	1 (5.0%)	0 (0.0%)	1 (5.0%)	0 (0.0%)	0 (0.0%)

[a]Only AEs with incidence ≥10% are shown (unless grade ≥2) [b]Adverse events reported occurred following FMT administration and prior initiation of immune checkpoint inhibitor (ICI) therapy. [c]Patient 101-025 (NSCLC) experienced a grade 4 increase in lipase levels, the symptoms were grade 1 abdominal pain with no abnormality on CT scan. [d]Adverse events reported occurred following FMT administration and prior initiation of immune checkpoint inhibitor (ICI) therapy. Patient 101-011 (Cutaneous melanoma) experienced a heart attack, which resulted in death. This incident was reported outside of the designated reporting period. The event was reviewed by the Data Safety Monitoring Board which concluded that it was not related to FMT or ICI.

nature portfolio

Corresponding author(s): Arielle Elkrief

Last updated by author(s): Dec 2, 2025

Reporting Summary

Nature Portfolio wishes to improve the reproducibility of the work that we publish. This form provides structure for consistency and transparency in reporting. For further information on Nature Portfolio policies, see our Editorial Policies and the Editorial Policy Checklist.

Statistics

For all statistical analyses, confirm that the following items are present in the figure legend, table legend, main text, or Methods section.

n/a	Confirmed
☐	☒ The exact sample size (*n*) for each experimental group/condition, given as a discrete number and unit of measurement
☐	☒ A statement on whether measurements were taken from distinct samples or whether the same sample was measured repeatedly
☐	☒ The statistical test(s) used AND whether they are one- or two-sided *Only common tests should be described solely by name; describe more complex techniques in the Methods section.*
☐	☒ A description of all covariates tested
☐	☒ A description of any assumptions or corrections, such as tests of normality and adjustment for multiple comparisons
☐	☒ A full description of the statistical parameters including central tendency (e.g. means) or other basic estimates (e.g. regression coefficient) AND variation (e.g. standard deviation) or associated estimates of uncertainty (e.g. confidence intervals)
☐	☒ For null hypothesis testing, the test statistic (e.g. *F*, *t*, *r*) with confidence intervals, effect sizes, degrees of freedom and *P* value noted *Give P values as exact values whenever suitable.*
☒	☐ For Bayesian analysis, information on the choice of priors and Markov chain Monte Carlo settings
☒	☐ For hierarchical and complex designs, identification of the appropriate level for tests and full reporting of outcomes
☐	☒ Estimates of effect sizes (e.g. Cohen's *d*, Pearson's *r*), indicating how they were calculated

Our web collection on statistics for biologists contains articles on many of the points above.

Software and code

Policy information about availability of computer code

Data collection	For shotgun metagenomics, data is publicaly available at the NCBI repository posted in the manuscript. The tumor sizes were measured throughout the experiment using a caliper. Two-dimensional measurements (HxL) were performed. For the flow cytometry, the stained cells were acquired using Cytek Aurora 5-laser spectral analyzer for human PBMCs.
Data analysis	GraphPad Prism (version 10.4.2) was used for the generating Fig(s) 4G-J, 5C-G, Extended Figure(s) 5C-D, 6B-D, 7 E-F, 8A. Microbiome sequencing data were processed and analyzed using the phyloseq package (v.1.50.0). Alpha diversity analysis was performed using the vegan package (v.2.7.1). Principal component analysis was done with the packages prcomp (v.4.4.2), and factoextra (v.1.0.7). PERMANOVA analysis was performed with 999 permutations using the adonis function from the vegan package. Strain sharing between the patients and donors was calculated using StrainPhlAn4 with an in-house database for strain identification as previously published. Bray-Curtis dissimilarity was calculated between the samples and their corresponding donor samples using the distance function from phyloseq. Linear discriminant analysis Effect Size (LEfSe) was performed to identify microbial taxa that differentiate between subject groups according to their response, cohort or toxicity development using the package yingtools2 (v.0.0.1.184). Taxonomic abundance patterns between groups were visualized via heatmaps generated by the ComplexHeatmap package (v.2.22.0). Shotgun metagenomic samples were also processed with the HMP Unified Metabolic Analysis Network (HUMAnN3) pipeline (v.3.8). Differential abundance analysis between baseline and post-FMT was performed using DESeq2 (v.1.46.0).

For manuscripts utilizing custom algorithms or software that are central to the research but not yet described in published literature, software must be made available to editors and reviewers. We strongly encourage code deposition in a community repository (e.g. GitHub). See the Nature Portfolio guidelines for submitting code & software for further information.

Data

Policy information about availability of data

All manuscripts must include a data availability statement. This statement should provide the following information, where applicable:

- Accession codes, unique identifiers, or web links for publicly available datasets
- A description of any restrictions on data availability
- For clinical datasets or third party data, please ensure that the statement adheres to our policy

Raw fastq files are publicly available on the NCBI biorepository with accession number PRJNA1289847. Individual patient data will be made available upon request to the corresponding author with data sharing agreement.

Research involving human participants, their data, or biological material

Policy information about studies with human participants or human data. See also policy information about sex, gender (identity/presentation), and sexual orientation and race, ethnicity and racism.

Reporting on sex and gender	Biological sex was considered in the study and we had 60% male and 40% female participants. Gender was not considered in the study.
Reporting on race, ethnicity, or other socially relevant groupings	Donor race and ethnicity is included in Extended Data Table 1.
Population characteristics	Population characteristics is included in Extended Data Table 2.
Recruitment	Recruitment: Patients were enrolled and treated at five academic centers in Canada: Centre Hopitalier de l'Université de Montréal (CHUM; Québec), the London Regional Cancer Program (LRCP; Ontario), Centre hospitalier de l'Université de Québec (CHUQ; Québec), McGill University Health Centre (MUHC; Québec), Lakeridge Health (Oshawa; Ontario). Patients were recruited by their treating oncologist or a member of the research unit authorized to review patients with the treating oncologist. Patients were provided with a verbal outline of the trial followed by a copy of the consent dorm to review, Written informed consent was obtained by a co-investigator.
Ethics oversight	The clinical trial and correlative analyses were approved by the CHUM Ethics Review Board and each participating centre, ethics number: MP-02-2022-10121/21.173. For culturomics analysis, this was conducted under project number: 2025-12377 through biobank numbers MP-02-2018-7132/17.035 and 16.161.

Note that full information on the approval of the study protocol must also be provided in the manuscript.

Field-specific reporting

Please select the one below that is the best fit for your research. If you are not sure, read the appropriate sections before making your selection.

☒ Life sciences ☐ Behavioural & social sciences ☐ Ecological, evolutionary & environmental sciences

For a reference copy of the document with all sections, see nature.com/documents/nr-reporting-summary-flat.pdf

Life sciences study design

All studies must disclose on these points even when the disclosure is negative.

Sample size	n=20 NSCLC and 20 melanoma patients. For the NSCLC cohort, assuming that the ORR rate is 39% (null hypothesis), a sample size of 18 patients with has 80% to detect an ORR of 64% (alternative hypothesis) using a one-sided binomial test with 0.10 level of significance. Since the pre-specified primary endpoint of the study was ORR in the NSCLC cohort, there was no pre-specified sample size calculation for the cutaneous melanoma cohort. For mice experiments, groups of 10 mice per condition were used, ensuring statistical power while minimizing animal use.
Data exclusions	Specific sub-group analyses were included in the methods
Replication	Mouse experiments were reproduced in two independent experiments.
Randomization	The clinical trial was not randomized. Mice underwent randomisation as stated in the methods.
Blinding	Blinding is not applicable since the clinical trial was not blinded.

Reporting for specific materials, systems and methods

We require information from authors about some types of materials, experimental systems and methods used in many studies. Here, indicate whether each material, system or method listed is relevant to your study. If you are not sure if a list item applies to your research, read the appropriate section before selecting a response.

Materials & experimental systems

n/a	Involved in the study
☐	☒ Antibodies
☐	☒ Eukaryotic cell lines
☒	☐ Palaeontology and archaeology
☐	☒ Animals and other organisms
☐	☒ Clinical data
☒	☐ Dual use research of concern
☒	☐ Plants

Methods

n/a	Involved in the study
☒	☐ ChIP-seq
☐	☒ Flow cytometry
☒	☐ MRI-based neuroimaging

Antibodies

Antibodies used

Antibodies for flow cytometry including dilution factors were detailed in Methods section and in the provided supplemental tables. For mouse experiments: anti-PD-1 monoclonal antibody (250 µg per mouse; clone RMP1-14, Bio X Cell) or isotype control (clone 2A3, Bio X Cell) were used in this study. The antibodies were purchased from the supplier Cedarlane.

Validation

For flow cytometry antibodies (Human experiments):
https://www.thermofisher.com/order/catalog/product/L23105
https://www.bdbiosciences.com/en-ca/products/reagents/flow-cytometry-reagents/research-reagents/buffers-and-supporting-reagents-ruo/brilliant-stain-buffer-plus.566385?tab=product_details
https://www.biolegend.com/de-de/products/brilliant-violet-510-streptavidin-8140
https://www.bdbiosciences.com/en-ca/products/reagents/flow-cytometry-reagents/research-reagents/single-color-antibodies-ruo/bv605-mouse-anti-human-cd194.562906?tab=product_details
https://www.bdbiosciences.com/en-ca/products/reagents/flow-cytometry-reagents/research-reagents/single-color-antibodies-ruo/buv661-mouse-anti-human-cd196-ccr6.569509?tab=product_details
https://www.bdbiosciences.com/en-ca/products/reagents/flow-cytometry-reagents/research-reagents/single-color-antibodies-ruo/buv737-mouse-anti-human-ccr7-cd197.749676?tab=product_details
https://www.biolegend.com/de-de/products/pe-dazzle-594-anti-human-cd199-ccr9-antibody-14763
https://www.biolegend.com/de-de/products/brilliant-violet-570-anti-mouse-human-cd11b-antibody-7380
https://www.biolegend.com/de-de/products/alexa-fluor-647-anti-human-cd123-antibody-8525
https://www.bdbiosciences.com/en-ca/products/reagents/flow-cytometry-reagents/research-reagents/single-color-antibodies-ruo/r718-mouse-anti-human-cd127.566967?tab=product_details
https://www.biolegend.com/de-de/products/spark-blue-550-anti-human-cd14-antibody-18496
https://www.biolegend.com/de-de/products/brilliant-violet-421-anti-human-cd141-thrombomodulin-antibody-9130
https://www.bdbiosciences.com/en-ca/products/reagents/flow-cytometry-reagents/research-reagents/single-color-antibodies-ruo/buv805-mouse-anti-human-cd16.569165?tab=product_details
https://www.biolegend.com/de-de/products/apc-anti-human-cd163-antibody-6276
https://www.bdbiosciences.com/en-ca/products/reagents/flow-cytometry-reagents/research-reagents/single-color-antibodies-ruo/bb515-mouse-anti-human-siglec-1-cd169.565353?tab=product_details
https://www.biolegend.com/de-de/products/pefire-640-anti-human-cd19-antibody-19533
https://www.bdbiosciences.com/en-ca/products/reagents/flow-cytometry-reagents/research-reagents/single-color-antibodies-ruo/bv480-mouse-anti-human-cd1c.746677?tab=product_details
https://www.biolegend.com/de-de/products/percp-cyanine5-5-anti-human-cd206-mmr-antibody-7404
https://www.biolegend.com/de-de/products/pefire-700-anti-human-cd25-antibody-19788
https://www.biolegend.com/de-de/products/brilliant-violet-650-anti-human-cd3-antibody-13475
https://www.biolegend.com/de-de/products/pe-anti-human-cd301-clec10a-antibody-7914
https://cytekbio.com/products/cfluor-568-anti-human-cd4?variant=32351881986084
https://www.biolegend.com/de-de/products/brilliant-violet-650-anti-human-cd40-antibody-12322
https://www.biolegend.com/de-de/products/percp-anti-human-cd45-antibody-12393
https://www.bdbiosciences.com/en-ca/products/reagents/flow-cytometry-reagents/research-reagents/single-color-antibodies-ruo/buv395-mouse-anti-human-cd45ra.740298?tab=product_details
https://www.bdbiosciences.com/en-ca/products/reagents/flow-cytometry-reagents/research-reagents/single-color-antibodies-ruo/buv563-mouse-anti-human-cd5.741354?tab=product_details
https://www.biolegend.com/de-de/products/spark-nir-685-anti-human-cd69-antibody-20086
https://www.biolegend.com/de-de/products/apc-fire-810-anti-human-cd8-antibody-19536
https://www.bdbiosciences.com/en-ca/products/reagents/flow-cytometry-reagents/research-reagents/single-color-antibodies-ruo/bv786-mouse-anti-human-cd86.740990?tab=product_details
https://www.biolegend.com/de-de/products/apc-fire-750-anti-human-cd88-c5ar-antibody-16464
https://www.bdbiosciences.com/en-ca/products/reagents/flow-cytometry-reagents/research-reagents/single-color-antibodies-ruo/buv496-mouse-anti-human-cd89.750617?tab=product_details
https://www.thermofisher.com/antibody/product/CD152-CTLA-4-Antibody-clone-14D3-Monoclonal/46-1529-42
https://www.bdbiosciences.com/en-ca/products/reagents/flow-cytometry-reagents/research-reagents/single-color-antibodies-ruo/pe-cy-7-mouse-anti-human-cd183.560831?tab=product_details
https://www.bdbiosciences.com/en-ca/products/reagents/flow-cytometry-reagents/research-reagents/single-color-antibodies-ruo/buv615-rat-anti-human-cxcr5-cd185.751293?tab=product_details
https://www.bdbiosciences.com/en-ca/products/reagents/flow-cytometry-reagents/research-reagents/single-color-antibodies-ruo/bv711-mouse-anti-human-fc-r1.747783?tab=product_details

https://www.biolegend.com/de-de/products/pe-fire-810-anti-human-hla-dr-antibody-21104
https://www.rndsystems.com/products/human-integrin-alpha4beta7-lpam-1-research-grade-vedolizumab-biosimilar-alexa-fluor-405-conjugated-antibody-hu117_fab10078v
https://www.bdbiosciences.com/en-ca/products/reagents/flow-cytometry-reagents/research-reagents/single-color-antibodies-ruo/bv750-mouse-anti-human-cd279-pd-1.747446?tab=product_details
https://www.thermofisher.com/antibody/product/CD274-PD-L1-B7-H1-Antibody-clone-MIH1-Monoclonal/15-5983-42
https://www.miltenyibiotec.com/CA-en/products/slan-m-dc8-antibody-anti-human-dd-1.html

Eukaryotic cell lines

Policy information about cell lines and Sex and Gender in Research

Cell line source(s)	MCA-205: a mouse fibrosarcoma cell line synergenic to C57BL/6 mice. Provided by Dr. John Stagg from CRCHUM Montreal
Authentication	The cell lines were authenticated by IDEXX BioResearch through PCR assay.
Mycoplasma contamination	Cell lines were checked for mycoplasma using PlasmoTest Mycoplasma Detection Kit (InvivoGen).
Commonly misidentified lines (See ICLAC register)	No commonly misidentified cell lines from the ICLAC register were used in this study.

Animals and other research organisms

Policy information about studies involving animals; ARRIVE guidelines recommended for reporting animal research, and Sex and Gender in Research

Laboratory animals	Murine experiments were conducted using seven-week-old female wild type C57BL/6 mice, obtained from Charles River and maintained at the Centre de recherche du Centre hospitalier de l'Université de Montréal (CRCHUM) GF Facility. All mice were 6-8 weeks old for this study.
Wild animals	Not applicable.
Reporting on sex	Female mice were used.
Field-collected samples	Not applicable.
Ethics oversight	All animal studies were approved by the Institutional Animal Care Comimittee (CIPA) and carried out in compliance with the Canadian Council on Animal Care guidelines. Ethical number: C22017Br.

Note that full information on the approval of the study protocol must also be provided in the manuscript.

Clinical data

Policy information about clinical studies

All manuscripts should comply with the ICMJE guidelines for publication of clinical research and a completed CONSORT checklist must be included with all submissions.

Clinical trial registration	NCT04951583
Study protocol	The study protocol is included in the submission.
Data collection	Medidata Rave EDC. Samples were collected from patient enrolled in the trial from six centres across Canada.
Outcomes	Primary and secondary outcomes are stated in the methods. For the NSCLC cohort, assuming that the ORR rate is 39% (null hypothesis), a sample size of 18 patients with has 80% to detect an ORR of 64% (alternative hypothesis) using a one-sided binomial test with 0.10 level of significance. Since the pre-specified primary endpoint of the study was ORR in the NSCLC cohort, there was no pre-specified sample size calculation for the cutaneous melanoma cohort.

Plants

Seed stocks — *Report on the source of all seed stocks or other plant material used. If applicable, state the seed stock centre and catalogue number. If plant specimens were collected from the field, describe the collection location, date and sampling procedures.*

Novel plant genotypes — *Describe the methods by which all novel plant genotypes were produced. This includes those generated by transgenic approaches, gene editing, chemical/radiation-based mutagenesis and hybridization. For transgenic lines, describe the transformation method, the number of independent lines analyzed and the generation upon which experiments were performed. For gene-edited lines, describe the editor used, the endogenous sequence targeted for editing, the targeting guide RNA sequence (if applicable) and how the editor was applied.*

Authentication — *Describe any authentication procedures for each seed stock used or novel genotype generated. Describe any experiments used to assess the effect of a mutation and, where applicable, how potential secondary effects (e.g. second site T-DNA insertions, mosiacism, off-target gene editing) were examined.*

Flow Cytometry

Plots

Confirm that:

☒ The axis labels state the marker and fluorochrome used (e.g. CD4-FITC).

☒ The axis scales are clearly visible. Include numbers along axes only for bottom left plot of group (a 'group' is an analysis of identical markers).

☒ All plots are contour plots with outliers or pseudocolor plots.

☒ A numerical value for number of cells or percentage (with statistics) is provided.

Methodology

Sample preparation — Cryopreserved peripheral blood mononuclear cells (PBMCs) from NSCLC patients undergoing combined anti-PD-1 and FMT and melanoma patients undergoing combined anti-PD-1+anti-CTLA-4 and FMT were thawed, washed and resuspended in complete RPMI medium. One million cells were labelled for viability with LIVE/DEAD™ Fixable Blue Dead Cell Stain (Invitrogen) (30min, room temperature). Fc blocking antibody was added to cells to decrease non-specific binding and background fluroscence (10min, 4 deg C) and intracellular markers (30mins, room temperature).

Instrument — Flow Cytometry data was acquired using a Cytek Aurora 5-laser spectral analyzer

Software — BD FACSDiva Software was used during the stained cells in the cytometer.
Flow cytometry raw data anlysis were performed with FlowJo v10.8.1

Cell population abundance — One million cells were labelled for viability with LIVE/DEAD™ Fixable Blue Dead Cell Stain (Invitrogen) (30min, room temperature). Fc blocking antibody was added to cells to decrease non-specific binding and background fluroscence (10min, 4 deg C) and intracellular markers (30mins, room temperature) (Extended Data Table).

Gating strategy — Gating strategy: The gating strategy for the human PBMC staining are provided in Extended Figure 8.

☒ Tick this box to confirm that a figure exemplifying the gating strategy is provided in the Supplementary Information.